

REPORT DOCUMENTATION PAGE

Form Approved
OMB No. 0704-0188

Public reporting burden for this collection of information is estimated to average 1 hour per response, including the time for reviewing instructions, searching existing data sources, gathering and maintaining the data needed, and completing and reviewing the collection of information. Send comments regarding this burden estimate or any other aspect of the collection of information, including suggestions for reducing this burden, to Washington Headquarters Services, Directorate for Information Operations and Reports, 1215 Jefferson Davis Highway, Suite 1204, Arlington, VA 22202-4302, and to the Office of Management and Budget, Paperwork Reduction Project (0704-0188), Washington, DC 20503

1. AGENCY USE ONLY (Leave blank)		2. REPORT DATE April 1992	3. REPORT TYPE AND DATES COVERED Final - 6/89-6/92	
4. TITLE AND SUBTITLE Microwave Interactions with Plasmas			5. FUNDING NUMBERS Contract No. F49620-90-C-0041	
6. AUTHOR(S) D. J. Eckstrom, R. J. Vidmar, K. R. Stalder				
7. PERFORMING ORGANIZATION NAME(S) AND ADDRESS(ES) SRI International 333 Ravenswood Avenue Menlo Park, CA 94025-3493			8. PERFORMING ORGANIZATION REPORT NUMBER Project 1261 MP 92-011	
9. SPONSORING/MONITORING AGENCY NAME(S) AND ADDRESS(ES) Air Force Office of Scientific Research Bolling AFB, DC 20332-6448			10. SPONSORING/MONITORING AGENCY REPORT NUMBER MP 2301 A8	
11. SUPPLEMENTARY NOTES				
12a. DISTRIBUTION/AVAILABILITY STATEMENT Distribution unlimited			12b. DISTRIBUTION CODE	
13. ABSTRACT (Maximum 200 words) Microwave interactions with a cold, collisional plasma having gradual density gradients were studied. The plasma was created by the photoionization of tetrakisdimethylaminoethylene (TMAE) vapor seeded into atmospheric pressure helium. Photoionization was provided primarily by sparkboards. Spatial scans of the absorption of a microwave probe beam along chords across the plasma, with subsequent Abel inversion, yielded three-dimensional plasma density profiles that showed a gradual decrease in the peak plasma density versus distance away from the sparkboard. When a 58-cm-diameter reflector was illuminated with 10-GHz microwaves in an anechoic chamber, the plasma absorbed as much as 28 dB in direct reflection, with similar attenuation of the normally weak side-scattered and cross-polarized radiation. The attenuation was compared with model predictions. Detailed analysis of the temporal and spatial dependence of the electron density following ionization indicates that both recombination and attachment processes influenced the plasma decay. The recombination rate of TMAE was found to be $(9.0 \pm 1.1) \times 10^{-6} \text{ cm}^3 \text{ s}^{-1}$ for 300 K electrons. This work confirms the effectiveness of a cold, collisional plasma as a broadband, switchable microwave absorber.				
14. SUBJECT TERMS Plasmas, Microwave-Plasma Interactions, Microwave Absorption, Afterglows			15. NUMBER OF PAGES 69 Incl. Append.	
			16. PRICE CODE	
17. SECURITY CLASSIFICATION OF REPORT Unclassified	18. SECURITY CLASSIFICATION OF THIS PAGE Unclassified	19. SECURITY CLASSIFICATION OF ABSTRACT Unclassified	20. LIMITATION OF ABSTRACT None	

CONTENTS

SUMMARY.....	1
PRINCIPAL RESEARCH FINDINGS.....	3
Task 1: Plasma Production Methods.....	3
Task 2: Characterization Methods.....	6
Task 3: Experimental Measurements.....	7
Task 4: Modeling.....	8
CONCLUSION AND RECOMMENDATIONS	9

APPENDICES

- A Preprint, "Observations of Strong Microwave Absorption in Collisional Plasmas with Gradual Density Gradients," K. R. Stalder, R. J. Vidmar, and D. J. Eckstrom, submitted to J. Appl. Phys. (1992).
- P Preprint, "Afterglow Decay Kinetics of Non-Uniform Plasmas with Cylindrical Symmetry: Application to the Measurement of Plasma Decay in Large, Photoionized Plasmas in Atmospheric-Pressure Helium," K. R. Stalder and D. J. Eckstrom, submitted to J. Appl. Phys. (1992).
- C Abstract, "Investigations of Efficient Photoionization Methods for Creating Highly Collisional Plasmas," K. R. Stalder, D. J. Eckstrom and R. J. Vidmar. Presented at the 43rd Annual Gaseous Electronics Conference, Champaign-Urbana, IL, 16-19 October 1990.
- D Abstract, "Microwave-Plasma Interactions in Photoionized, TMAE-seeded Helium Gas Mixtures," K. R. Stalder, D. J. Eckstrom and R. J. Vidmar. Presented at the 1991 IEEE International Conference on Plasma Science, Williamsburg, VA, 3-5 June, 1991
- E Abstract, "Dissociative Recombination of TMAE Ions," K. R. Stalder, D. J. Eckstrom and R. J. Vidmar. Presented at the 44th Annual Gaseous Electronics Conference, Albuquerque, NM, 22-25 October 1991
- F Abstract, "Microwave Absorption Characteristics of an Atmospheric-Pressure, Photoionized Plasma," K. R. Stalder, D. J. Eckstrom, and R. J. Vidmar. Presented at the 1991 Annual Meeting of the APS Division of Plasma Physics, Tampa FL, 4-8 November 1991. Also published in Bull. Am. Phys. Soc., 36, 2485 (1991).



By	
Dist istribution /	
Availability Codes	
Dist	Avail and/or Special
A-1	



SUMMARY

The primary objectives of this research were to investigate methods of producing plasmas with microwave absorptive properties and to quantify those properties using several diagnostic techniques, including microwave interferometry, Langmuir probes, and radar reflectivity measurements. This work was motivated by recent modeling work by R. J. Vidmar* suggesting that dense collisional plasmas may be useful for a variety of electromagnetic applications, especially those related to radar attenuation.

Methods of generating a microwave-absorbing plasma centered on photoionization of a seed gas in an inert buffer gas. Several photoionization schemes were investigated and compared on the basis of efficiency, cost, and availability. We concentrated on sparkboard discharges for the photoionization light sources based on available components. Some limited experiments using alternative photoionization sources, namely, flashlamps, were tried briefly, but the sparkboard was found to produce higher plasma densities.

The ionization medium consisted of a low ionization potential molecule, tetrakisdimethylaminoethylene (TMAE), seeded into atmospheric pressure helium. Used with the sparkboard source, this combination allowed us to generate significant plasma densities that were highly collisional and that extended for tens of centimeters, thus creating an effective plasma absorber for 10-GHz microwaves. Experimentally, we found that absorption of microwave probe beams (closely related to interferometric techniques) was a sensitive way to measure plasma density profiles. Using this technique, we determined the electron density, the three-dimensional distribution of the plasma, and many aspects of the plasma decay mechanisms. Typical electron densities on the sparkboard centerline exceeded $n_e \sim 2 \times 10^{11} \text{ cm}^{-3}$ at a distance of 7 cm from the surface.

Plasma lifetimes were expected to be controlled by electron recombination and attachment. Diagnostic techniques and models were developed to describe the temporal and spatial behavior of the plasma. Experimentally, the plasma persisted for tens of microseconds following cessation of light from the sparkboard. We confirmed that these kinetic effects controlled the decay, and we measured the rate constants that describe the recombination of TMAE.

Validation experiments were conducted in a high-dynamic-range microwave absorber tunnel to quantify the absorption characteristics of the plasma. The highest peak attenuation of

* R. J. Vidmar, IEEE Trans. Plasma Sci. **18**, 733 (1990)

Validation experiments were conducted in a high-dynamic-range microwave absorber tunnel to quantify the absorption characteristics of the plasma. The highest peak attenuation of directly backscattered 10-GHz radiation was 28 dB. There was no significant bistatic scattering or polarity rotation of the 10-GHz radiation. These reductions in backscattered microwave intensity were achieved from a large circular reflecting target of 58 cm diameter. This level of performance was a significant improvement over other experiments using smaller targets.

Experimental difficulties prevented us from measuring the electron density profile near the surface of the sparkboards. This incomplete knowledge of the profile, together with the three-dimensional shape of the plasma contours, precludes a detailed comparison between experiments and our existing one-dimensional theory, although an approximate prediction agrees well with the measurement.

The research did identify several aspects of plasma absorber technology requiring further effort, including engineering development of more compact and efficient ionization sources, identification of more efficient ionization media, and development of better gas purification techniques. Successful completion of those efforts will make possible practical applications of strongly absorbing plasma media.

PRINCIPAL RESEARCH FINDINGS

We describe the major results of our research here in the same order as in our revised Statement of Work. Many of the details, with references, are covered in the manuscripts of the two papers submitted for publication, Appendices A and B. Appendices C through F are abstracts of conference papers presented during this contract.

TASK 1: PLASMA PRODUCTION METHODS

Under Task 1, we were to investigate means of producing plasmas with appropriate density and collisionality such that they would be effective microwave absorbers. We proposed that we would investigate bare flashboards (sparkboards) or flashlamps or, if required, electron beam ionization of high pressure gas.

We chose to concentrate on sparkboard technology for the ionization source. This choice was motivated by our significant prior experience in understanding the ionization characteristics of the candidate sources and by considering many aspects of the desired specifications that a practical system would require. Since sparkboards have been used in many applications where large volumes of photoionized plasma are required, such as large CO₂ laser systems, and since many of the requirements for plasma absorbers have similar features, this choice seemed logical. These requirements include compactness, overall efficiency of producing photoionizing photon fluxes (i.e., intense light in UV and VUV spectral ranges), and scalability to larger sizes.

In conjunction with our choice of photoionization source, we chose to use a low ionization potential seed gas, tetrakisdimethylaminoethylene (TMAE), an organic molecule having a significant vapor pressure at room temperature. Previous research by us and others indicated that this molecule might have significant promise as an ionization media. We chose to seed the TMAE into atmospheric pressure helium because helium offers the longest plasma lifetime of any buffer gas. Furthermore, the electron collision frequency in helium is well known and the spectral emission from sparks generated in it is known to include wavelengths that produce strong ionization of TMAE.

All our research was conducted in an experimental apparatus designed for further testing in a microwave anechoic chamber (see Task 3, below). This required us to conduct experiments in plastic enclosures that had low microwave backscattering and yet enabled us to maintain adequate

gas purity. Because the plastic would tear if the plasma region were pumped, we were unable to pump on the enclosure to remove oxygen and other deleterious impurities.

Using pulsed-power components from an old flashlamp-pumped dye laser (Candela Corp. Model TFDL-1), we constructed a 110-joule capacitor bank and switching circuit for driving the pulsed sparkboard light source. The 0.3- μ F capacitor in this power source was charged by a 0-to-30 kV DC power supply (Universal Voltronics) and was triggered with an EG&G HY-05 Thyatron. The stored energy was discharged into the sparkboard through low inductance current leads. Each sparkboard was constructed from an ordinary printed circuit board that was etched with appropriate patterns to form 30 planar sparkgaps in 5 parallel current paths.

Initial experiments were conducted with just one sparkboard mounted on the power source. We measured the voltage-current characteristics of the planar-surface discharge and found it to be well represented by a damped, oscillating discharge. Typically lasting 3-5 μ s, the discharge rang with a 1 μ s period and was damped in 3 to 5 cycles. The peak current was as high as 10 kA. The phase angle between the voltage and current was close to 90°, so the discharge was not critically damped and therefore only a fraction of the electrical energy was deposited in the discharge. Even with this circuit, significant volumes of photoionized plasma were produced. Optimization would increase the electrical efficiency of the source.

We then mounted the sparkboard on a 2-foot-diameter (58 cm) aluminum reflector. Many tests were conducted with just one sparkboard discharging up to 110 joules. After some diagnostic tests (described further in Task 2, below), it became apparent that one sparkboard would not produce the required plasma density and volume over enough of the reflector to cause a significant reduction in backscattered microwave radiation, as measured in Task 3. We therefore introduced four sparkboards, each identical to the first, wired in parallel. The configuration resembled a cross; the center of the cross consisted of a square oxygen-free high-conductivity (OFHC) copper plate that acted as a low inductance current feed to the four boards. The current to the copper plate was conducted through a coaxial feedthrough in the aluminum reflector plate. Return currents from the four boards flowed through a large cross-shaped low-inductance copper sheet, mounted directly below the sparkboards, and then flowed through the outer conductor of the coaxial feedthrough back to the power source.

A plastic (polyethylene) garbage bag served as our initial helium confinement vessel. It was thin and of the appropriate size to fit on the reflector base. Gas purity in these initial tests was achieved by continuously purging the bag with helium. Eventually, oxygen in the bag was replaced by helium, and except for outgassing from the bag, we were able to achieve modest gas purity levels quickly because the bags had numerous pinholes to let out the residual impurities

along with the helium. When it became apparent that a lower level of impurities was required, we used a custom-built polyester film (Mylar) membrane in the shape of a conical frustrum. Originally developed by R. J. Vidmar as a low radar cross section support for large test structures for microwave testing, these membranes were useful in our research because their impermeability and leak-tightness to helium were vastly superior to the garbage bags. The small leakdown rate of the membrane still required continuous pressurization with high purity (99.995%) helium that was passed through an oxygen-absorbing purifier (Matheson Gas, Model 6412).

Just as with the garbage bags, however, pumping on the Mylar enclosure was not possible, so an improved gas purifying system was required. We developed a custom zeolite-based sorption pump that effectively removed oxygen and other impurities from the bag. The design was based on forcing helium through a densely packed column of A5 zeolite that was cooled to liquid nitrogen temperatures by a cold finger that conducted heat efficiently from an external liquid nitrogen bath to the interior of the pump. The zeolite side of the cold finger consisted of many vanes of OFHC copper, all soldered to a single 1-inch-diameter (2.5 cm) solid copper rod that passed through a vacuum feedthrough. Immersion of the copper rod in a bucket of liquid nitrogen then cooled the zeolite to temperatures where it effectively absorbed oxygen and other impurities while passing the helium. Gas was forced through the zeolite by a fan placed directly upstream of it. Valves were installed such that the sorption pump could be isolated and purged. Heating the isolated pump with heat-tapes while either venting it to air or pumping on it with a mechanical pump then removed the trapped gases. A series of pump-purge cycles lasting several days then allowed the gas in the membrane to achieve the purity level required for efficient plasma production and experimentation. Once the helium was sufficiently pure, TMAE was introduced by bubbling ultra-high pure helium through a temperature-controlled TMAE reservoir and into the confinement vessel.

Several brief experiments were conducted using high energy flashlamps. In previous independent research, we had studied the photoionization characteristics of TMAE-seeded helium in an L-band waveguide. The short-arc flashlamp (EG&G Electro-Optics, Model FX-193) used in those experiments discharged up to 7 joules in 10 μ s. It had a sapphire window for enhanced UV output. The light from the flashlamp passed through a 0.5-inch-thick (1.3 cm) Suprasil window and illuminated the interior of the waveguide. The results from those experiments indicated that electron densities of $2 \times 10^{10} \text{ cm}^{-3}$ were achieved, and the scale length for the electron density gradient was estimated to be about 10 cm, leading to approximately 10 dB attenuation of the microwave power. Also tried in those experiments were high-energy photographic flashlamps (Kemlite Laboratories, Inc., Model MW8-Q-V) that had the UV-absorbing envelope removed. These larger flashlamps could discharge up to 2,400 joules in 3 ms when operated with a large power pack (Speedotron Corp., Model 2401A). Peak attenuations comparable to those of the

EG&G lamp were observed, although the duration of strong attenuation was longer for the photographic flashlamp because of its longer flash duration.

The smaller EG&G flashlamp was unavailable for the present experiments, so the high energy flash system was used exclusively. We replaced the single sparkboard with the flashlamp and brought power leads through the back of the reflector. After several pump-purge cycles to purify the gas, we conducted experiments to study the photoionization of TMAE using the large flashlamp. Low attenuation of the transverse microwave probe beam was observed, even with flashlamp energies as high as 2,400 joules, indicating relatively poor photoionization by this source. We thus conclude that the sparkboard source was superior to the high energy flashlamp, but were unable to verify that this was the case for the EG&G flashlamps or for other flashlamp sources.

TASK 2: CHARACTERIZATION METHODS

Task 2 was concerned with investigating methods of characterizing the plasma density profile and lifetime. This task ran concurrently with Task 1 because we needed to know if the sparkboard was functioning as anticipated.

Our principal diagnostic was an X-Band microwave interferometer whose probe beam easily penetrated the plastic skin of the confinement membrane. For a plasma in 1 atm He, attenuation dominates over the phase shift of the probe beam, so that attenuation gives an accurate measure of the line-integrated electron density along the microwave beam path. Suitable computer programs for Abel-inversion of the chord-wise integrated electron densities were developed to determine spatial electron density profiles. The microwave transmission method is thoroughly discussed in Appendix B.

Early on, we found it necessary to use a Faraday cage to shield the diagnostic instrumentation from the rather severe noise generated when the sparkboard fired. The kiloampere-sized currents flowing through the sparkboard and in the ground return lines easily disrupted sensitive electronics, so considerable effort was required to achieve noise-free measurements. (The EG&G flashlamp used in earlier work generated much less noise, although it also provided only a fraction of the photoionization energy of the sparkboard.)

In addition to the microwave absorption method, we tried to use a Langmuir probe to determine the electron density profile. If successful, this technique would have been a better way to characterize the plasma density profile than the Abel-inversion technique, although its accuracy in determining the absolute electron density is not as good as the microwave technique. However, we had trouble with the probe operating in the pulsed plasma environment. Although the theory

and practice of probe current collection in high pressure gases are well known, probes are usually used in steady-state or transient plasma environments with little noise. The noise generated when the sparkboard fired was directly coupled into the probe; hence it overwhelmed the probe electronics for times longer than the actual plasma lifetime. We were able to reduce the noise by covering the sparkboards with screen cages to minimize this coupling, but we could never shield all ground currents well enough to have confidence in the probe measurements.

TASK 3: EXPERIMENTAL MEASUREMENTS

This task entailed experimental measurements of the transmission, reflection, and bistatic scattering of a cylindrically symmetric plasma placed in an absorber tunnel. Previous internal support at SRI had led to the construction of a portable microwave anechoic chamber. This absorber tunnel was modified for this contract to provide room for large-angle scattering experiments; hence, the tunnel became L-shaped. Details of these experiments are presented in the paper in Appendix A.

We used the four-board plasma generation technique developed in Task 1 for these measurements. For these tests, the reflector with sparkboards, the pulsed-power supply, and the gas conditioning components were mounted such that the axis of the helium-filled bag was horizontal and the reflector was vertical. The reflector had a 3.7-meter radius of curvature and the tunnel was 3.7-meters long, so effective plane-wave illumination was achievable in the absence of scattering from the sparkboard or its associated circuitry. We determined experimentally that the overall dynamic range for backscatter measurements with this configuration was 60 dB.

Briefly restating results described in Appendix A, we observed 28 dB attenuation of 10-GHz radiation in direct backscattering from the reflector when the plasma was present. The bistatic scattering from the bare plate was smaller than the direct backscatter by approximately 30 dB at angles up to 60° from the normal. The bistatic backscatter was further reduced by 15-20 dB when the plasma fired, and we observed comparable decreases in the normally weak cross polarized scattering. These results substantially validated our expectations based on the diagnostic measurements performed in Task 2 and the calculations presented by Vidmar.*

We limited our measurements to 10 GHz. However, we believe that the plasma would be a significant absorber over much larger bandwidths, as predicted by Vidmar.

* R. J. Vidmar, IEEE Trans. Plasma Sci. 18, 733 (1990).

TASK 4: MODELING

Task 4, modeling, was performed as needed to support and validate the findings from Task 3. Although we did not have complete information on the electron density profile near the reflector, our one-dimensional theoretical model nevertheless predicted a plasma attenuation that was in good agreement with the measurements on the three-dimensional experimental plasma. We also modeled the effects of switching from helium to argon as the buffer gas. However, we did not have quantitative information on the change in ionizing radiation output as a function of gas composition. Although the collision frequency in argon is significantly lower than in helium and therefore should have improved the absorption, we in fact observed lower attenuation. We believe this occurs because the UV light intensity generated in a sparkboard discharge of an argon/helium mixture in argon is shifted more toward the red than helium discharges and thus produces less efficient photoionization.

In addition to modeling results for one-dimensional plasmas and predicting the normal-incidence microwave attenuation, we also did extensive modeling of the time-dependent behavior of cylindrically symmetric, Gaussian-density-profile plasmas. This modeling is thoroughly discussed in the paper in Appendix B.

CONCLUSION AND RECOMMENDATIONS

This research program has contributed a significant body of knowledge on the technology of microwave-plasma interactions: monostatic and bistatic absorption measurements, deionization rates, and reduction to practice of a complete plasma absorber system. We were able to achieve dense plasmas that provided overall reductions in reflected power from a 2-foot-diameter (58 cm) reflector amounting to 28 dB. This level of performance over such a large target was unparalleled in the AFOSR program. We were able to model the time-dependent decay of this plasma and thus determined some of the fundamental decay processes controlling the peak plasma densities and hence the absorptivity and lifetime of the plasma. These measurements and modeling largely validated what we expected. They allow us to quantify and predict future performance.

Although the physics of microwave absorption in collisional plasmas is relatively mature, as confirmed in these laboratory experiments, many development issues must be resolved before plasma absorber technology can be applied. The greatest need is for improvement of the overall efficiency and operating characteristics of ionization sources. We believe there is significant room for improvement of the sparkboard light source in terms of duty cycle, overall source efficiency, and noise generation. It remains to be determined whether optimized flashlamps (e.g., short-arc xenon lamps with MgF_2 windows) could be more advantageous than sparkboards. New VUV light sources, such as silent discharges, should also be studied. Finally, there may be significant potential to be found in improved ionization media, such as dense, low-ionization-potential cluster molecules.

Appendix A

**OBSERVATIONS OF STRONG MICROWAVE ABSORPTION IN COLLISIONAL
PLASMAS WITH GRADUAL DENSITY GRADIENTS**

K. R. Stalder, R. J. Vidmar, and D. J. Eckstrom

To be Submitted to J. Appl. Phys. (1992).

OBSERVATIONS OF STRONG MICROWAVE ABSORPTION IN COLLISIONAL PLASMAS WITH GRADUAL DENSITY GRADIENTS

K. R. Stalder,* R. J. Vidmar,** and D. J. Eckstrom*

*Molecular Physics Laboratory

**System Techniques Laboratory

SRI International

Menlo Park, CA 94025

PACS Numbers: 52.25.Sw, 52.70.Gw, 52.80.Mg, 84.40.Cb

ABSTRACT

Strong microwave absorption was observed when a 10-GHz source illuminated an underdense collisional plasma that had a density-gradient-scale length several wavelengths long. Significant reductions in angular scattering and cross-polarized components were also observed. These experiments confirm that absorption was the dominant process. The plasma was created by the photoionization of tetrakisdimethylaminoethylene (TMAE) molecules seeded into atmospheric-pressure helium. Sparkboard arrays provided the intense vacuum ultraviolet ionizing radiation. Plasma density profiles were measured using transverse scans of 9.7-GHz probe microwaves and were found to approximate an Epstein profile. The absorption at 10 GHz by this plasma was as large as 28 dB in direct backscattering and 15-20 dB when orthogonally polarized microwaves were launched and detected. The peak absorption scales with sparkboard energy in a way that suggests that electron-ion recombination is the dominant electron-loss mechanism at high plasma densities.

MP 92-012
January 24, 1992

INTRODUCTION

Vidmar¹ has proposed that the strong microwave absorption associated with highly collisional plasmas may be exploited in many modern applications, especially those related to radar attenuation. Historically, study of the absorptive and reflective properties of electromagnetic waves illuminating plasmas was driven by the need for understanding radio wave propagation in the natural ionosphere.² Recent studies of the creation of artificial ionospheric conditions for a variety of purposes have also generated renewed interest in the absorptive and reflective properties of collisional plasmas.^{3,4} Given the historical and modern interest in the interactions of electromagnetic waves with collisional plasmas, more detailed aspects of the phenomenology of absorption and reflection are needed. In addition, the methods for achieving dense, highly collisional plasmas require development.

This paper describes recent laboratory experiments on generating absorptive plasmas with density gradients that have scale lengths longer than the free-space wavelength of the incident waves. We first review general aspects of microwave reflectivity from plasmas. Second we describe the details of the experiment, including descriptions of the atmospheric-pressure confinement vessel and the photoionization source. We then describe properties of the plasmas generated in the experiment. Experiments on the absorption of normal-incidence microwaves are reported. Finally, the scaling of the expected maximum electron density and absorption with source energy is discussed and compared with experiment. We show that microwave power is strongly absorbed by this plasma and confirm that there is no scattering of normal incidence microwave energy in other directions or polarizations.

SECTION 1. REFLECTIVE PROPERTIES OF PLASMAS

A semi-infinite slab of homogeneous dielectric material has the normal-incidence reflection coefficient, R , and transmission coefficient, T , given by the Fresnel formulas:

$$R = [(n - 1)/(n + 1)]^2, \quad (1)$$

and

$$T = 4/(n + 1)^2 \quad (2)$$

where n is the index of refraction of the dielectric. If the slab is of finite extent, reflections from the second interface enhance or diminish the reflection, depending on the phase relationship between waves reflected from the second interface to waves reflected from the first interface. In plasmas with near-cutoff densities and sharp boundaries, the reflection coefficient is significant.⁵ For example, in a collisionless plasma with an electron density of $8 \times 10^{11} \text{ cm}^{-3}$, $n = 0.37$ and $R = 0.22$ at 10 GHz. In this case, the power reflected back to the source is -7 dB of the incident power. This high reflectivity is an advantage in applications requiring good reflectivity, but is deleterious in those that require strong absorption. A highly collisional plasma can produce strong absorption; however, even with large collision frequencies, the bandwidth over which strong absorption occurs is reduced if the plasma density gradient scale length is shorter than the wavelength of the incident wave.¹

One method of reducing the reflections from plasma interfaces and increasing the absorption bandwidth is to tailor the density gradient.¹ The general case of waves obliquely incident on inhomogeneous plasmas was treated by Budden.² In these cases, specification of the density profile is also required. A convenient one-dimensional density profile that leads to analytic formulas for R and T is due to Epstein.⁶ It has a monotonically increasing electron-density profile defined by

$$n(z) = n_0/[1 + \exp(-z/\sigma)] \quad (3)$$

where n_0 is the peak density, z is the distance along the density gradient vector and σ is a density scale length. Ref. 1 shows many parametric curves for the reflection and transmission coefficients from this special density profile for various collision frequencies, microwave frequencies, and density scale lengths.

SECTION 2. ATMOSPHERIC-PRESSURE CONFINEMENT SYSTEM

A diagram of the plasma apparatus is shown in Figure 1. Many details of the experimental apparatus have been described previously.⁷ The plasma was created by the photoionization of tetrakisdimethylaminoethylene (TMAE) vapor seeded in purified helium gas at 760 Torr. TMAE was chosen for its combination of low first-ionization potential (5.37 eV) and its significant vapor pressure (0.5 Torr at 298 K). Other organic molecules with slightly less favorable characteristics have been used as photoionization seedants in laser applications.⁸⁻¹¹ The atmospheric-pressure helium provided the high electron collision frequency of approximately $1.8 \times 10^{11} \text{ s}^{-1}$.

Oxygen and other impurities were removed because of their combined deleterious effects of electron attachment and absorption of vacuum ultraviolet (VUV) photons (both of which degrade the performance of the absorber). To measure the normal-incidence microwave attenuation by this plasma, we confined the helium-TMAE mixture by a polyester-film (2-mil thick Mylar) containment vessel in the shape of a truncated conical frustrum, with the larger base consisting of a concave aluminum reflector plate and the smaller end consisting of a styrofoam plug. This plug was encapsulated with a heat shrinkable film to prevent leakage of gas through the styrofoam. Because the thin-walled plastic vessel would tear if the plasma region were pumped out, we relied on a custom-built circulating sorption pump system using repeated pump-purge cycles to remove oxygen from the helium gas.

SECTION 3. SPARKBOARD PHOTOIONIZATION SOURCE

The intense VUV radiation from sparkboard arrays mounted just above the aluminum reflector photoionized the TMAE. Sparkboard arrays have been used in many applications requiring efficient photoionization of large volumes.^{12,13} The sparkboards were fabricated from standard printed-circuit board material cut into 14 cm × 17 cm pieces and etched to provide 5 parallel current paths, with each path containing 6 sparkgaps. Each strip was approximately 7 mm wide and the spark gaps were approximately 3 mm long, separated by 19 mm along the strip and 15 mm between strips. Grounded strips on the backplane prevented the sparks from lifting off the board.¹²

The pulsed-power system shown schematically in Figure 2 contained a capacitor bank with a total capacitance of 0.3 μ F charged to between 9 and 27 kV, corresponding to stored energies between 12 and 110 joules. For voltages below the lower threshold, incomplete spark generation limited the sparkboard performance. For voltages exceeding the upper limit, internal breakdown in feedthroughs and the capacitor bank occurred. Upon triggering the thyratron, the full capacitor bank voltage was applied to one side of the sparkboard and a progression of sparks propagated down each conducting strip that contained gaps. The return current was conducted along low inductance copper striplines. Because the driving circuit was not critically damped, the current and voltage on the sparkboard rang for several cycles, depending on the capacitor-bank energy, resulting in a light pulse with a 3-5 microseconds duration. The open-shutter photograph in Figure 3 shows a single sparkboard discharge.

Although the spectral distribution of the light from the discharge in these experiments was not measured, previous work indicates that the sparks generated in atmospheric-pressure helium produce strong continuum radiation, in addition to strong line radiation. The line radiation may originate from the helium gas or from impurities driven off the sparkboard.¹⁴ In addition to strong visible radiation, there should be significant energy radiated in the VUV region from approximately

50-100 nm.¹⁵⁻¹⁷ Photon energies corresponding to wavelengths below 230 nm can photoionize TMAE in a one-step process, thus providing the ionization source for this plasma.

SECTION 4. MEASUREMENTS OF PLASMA DENSITY PROFILES

Initial experiments focused on developing the sparkboard source and measuring plasma profiles and decay kinetics. They were conducted with the apparatus mounted vertically on a separate test stand, as depicted in Figure 1. We performed experiments with two configurations, first using a single sparkboard and later using four identical sparkboards connected in parallel.

The plasma profile was determined using a 9.7-GHz microwave absorption system. Microwave transmit and receive horns (6 dB gain) connected to waveguides were mounted on an optical rail system providing movement in horizontal and vertical planes. Repeated shots at the same sparkboard energy enabled us to assemble a set of time-resolved chord-integrated absorption histories, which were subsequently Abel-inverted using a Gaussian fitting function.^{7,18} The density profile was found to closely approximate a Gaussian shape in the horizontal plane, as shown in Figure 4. With 22 Joules discharged into a single sparkboard, the FWHM for the horizontal density profile at 7 cm from the sparkboard at the time for peak ionization was 16 cm. In this case, the peak electron density was determined to be $1.6 \times 10^{11} \text{ cm}^{-3}$.

Although this arrangement provided significant ionization above the center of the aluminum reflector, we anticipated that significant reduction in microwave reflection from outer regions of the reflector would require a greater plasma-surface coverage, so we also performed experiments with four sparkboards, connected in parallel by a low-inductance copper plate. The four boards formed a cross. The plasma density profile in the case of four boards was significantly broader, as shown in Figure 4.

Near the source, the plasma can deionize via a recombination process more quickly than at greater distances where the dominant mechanism shifts to attachment. These processes combine to

form a complex temporally and spatially varying electron density profile. Nevertheless, by using a nonlinear least-squares fit of the measured density profile to an Epstein profile, we could empirically determine the density scale length σ . Because of the complex two-dimensional array of sparks and difficulty in measuring microwave absorption close to the baseplate, accurate measurements or models of the density close to the reflector were difficult to construct. Using on-axis densities from the Abel-inverted transverse microwave absorption data, we determined the density scale length σ to be approximately 5.3 cm, or approximately two free-space wavelengths at 10 GHz. Off axis, the densities were lower, but the density scale lengths were approximately the same.

In Figure 5 we present predictions based on the Epstein model for the total attenuation of microwaves versus frequency for various peak plasma densities and density scale lengths of 5 cm. These calculations are compared with our experimental measurements in the next section.

SECTION 5. EXPERIMENTS ON THE ATTENUATION OF NORMAL INCIDENCE MICROWAVES

Experiments were conducted with the plasma source cantilevered from the back wall of a long, L-shaped anechoic chamber lined with microwave-absorbing wedges and pyramids (Rantec Corp., Model EHP-8), as shown in Figure 6. The pulsed-power components for the sparkboard source and the gas purification system were mounted just outside the chamber with all the electrical and gas coupling shielded by the aluminum reflector or by absorber pyramids. The 58-cm-diameter reflector was machined with a 3.7-meter radius of curvature to provide effective plane-wave illumination over the reflector surface by the microwave source located 3.7 meters away (the sparkboard arrays perturbed the plane-wave illumination to some extent). The overall dynamic range for measuring reflections, limited by residual scattering from the absorber material, was approximately 60 dB. Scattering from the styrofoam plug and the Mylar film was below that limit. The dynamic range was significantly greater than the measured reduction in reflected power due to the plasma, which ensured an accurate measurement of the inherent plasma-produced absorption.

For high dynamic range measurements, we used a Hewlett Packard 8672A synthesized signal generator operating at 10.0 GHz as the microwave source. The microwave energy was coupled into a 10-dB waveguide horn, and an E-H tuner minimized reflections back to the source. The polarization of the incident radiation was controlled by rotating the transmit horn. Microwaves propagated along the long axis of the anechoic chamber and reflected from the aluminum baseplate. A significant fraction of the incident power was scattered directly back toward the source, where it was collected by a second 10-dB horn located near the source antenna. We checked the direct coupling between the transmit and receive antenna and found it to be insignificant.

The received power was detected by a low-noise amplifier (Miteq, Model AMF-4S-082117-25) with 25-dB gain and an overall noise figure of 2.5 dB. This boosted microwave signal was monitored by a spectrum analyzer (Hewlett Packard, Model 8566B) locked to the transmitter frequency. We used a 3-MHz video bandwidth to measure the signals, thus limiting the time resolution to about 300 ns. This bandwidth was more than sufficient to measure the peak absorption and the decay of the attenuation. The video output of the spectrum analyzer was recorded with a digital storage oscilloscope (Tektronix, Model 2430A), and data were downloaded and stored on a personal computer (Compaq Portable II). All the electronic components were contained in a screen box, which minimized the effect of noise generated when the sparkboard fired.

A result from a typical direct backscattering measurement is shown in Figure 7. The vertical scale is logarithmic in this case, and the maximum reduction in incident power amounted to 28 dB or nearly a 1000-fold attenuation of the reflected power. Although our simple model is not directly applicable, as mentioned in the previous section, we believe the observed attenuation is reasonably consistent with predictions shown in Figure 5 using a gradient scale length σ of 5 cm and a peak density n_0 slightly in excess of $5 \times 10^{11} \text{ cm}^{-3}$. Because the plasma did not cover the entire reflector uniformly, the only way a 28-dB reduction could occur was for significant plasma

densities to extend completely out to the Mylar skin. If only the central portion of the reflector was covered, then we estimate that only 16 dB of attenuation was possible.

Angular scattering was measured by moving the reception horn to the side of the L-section. Because of the effective plane-wave illumination, angular scattering was significantly reduced from the direct backscatter. We found it necessary during these measurements to boost the source power, using traveling wave tube amplifiers (TWTA) (Hughes Model 1177 H03 or Varian Model VZM699). Figure 8 shows results from a progression of angular-scattering experiments at 0°, 45°, and 60°. These data show that even the weak sidelobe-power was significantly attenuated.

Polarization rotation was not expected in these experiments because the plasma source did not contain any polarization-changing elements. Nevertheless, we performed some experiments to examine the polarization rotation, that is, cross polarization coupling. We observed approximately 15-20 dB reductions in the cross-polarized radiation. No enhancements were ever observed. This included measurements with TE (electric field transverse to the plane of incidence) and TM (electric field parallel to the plane of incidence) polarizations.

SECTION 6. PEAK MICROWAVE ATTENUATION AND ITS RELATIONSHIP TO THE SPARKBOARD ENERGY

The plasma density is determined by the balance between photoionization and deionization as given by the equation

$$dn_e/dt = S^+ - \alpha'n_e^2 - \lambda'n_e \quad (4)$$

where S^+ represents the photoionization rate, α' is the effective electron-ion recombination rate coefficient, and λ' is the effective electron attachment frequency. For the conditions of this experiment, we previously reported⁷ that $\alpha' \sim 9 \times 10^{-6} \text{ cm}^3 \text{ s}^{-1}$ and $\lambda' \sim 10^5 \text{ s}^{-1}$. Thus, for electron densities significantly greater than 10^{10} cm^{-3} , the electron attachment rate is negligible with respect to the recombination rate.

The photoionization rate, S^+ , is dependent on the spectral intensity of the radiation from the sparkboard, $I(\lambda)$, as well as the photoionization cross section of TMAE, $\sigma(\lambda)$:

$$S^+ = \int I(\lambda)\sigma(\lambda)n_{\text{TMAE}}d\lambda \quad (5)$$

where λ is the wavelength of the ionizing radiation and n_{TMAE} is the density of TMAE molecules. Our photodiode measurements showed that the light intensity was at its maximum for times longer than the recombination time ($\tau_{\text{recom}} = \frac{1}{\alpha'n_e}$). Then the electron density is at quasi-steady state ($dn_e/dt = 0$) and the ionization rate balances the recombination rate ($S^+ \cong \alpha'n_e^2$). If discharge times were independent of capacitor-bank energy, the peak light intensity would be proportional to stored energy. Then the peak electron density should vary as the square-root of the sparkboard energy, E . The microwave attenuation measured in decibels is predicted to be linearly proportional to the maximum electron density.¹

We show the peak attenuation versus sparkboard energy in Figure 9. It is clear that the attenuation obeys a power law dependence; in this case $A(\text{dB}) \propto E^{0.37}$. An explanation for the departure from exact square-root dependence is that greater capacitor-bank energies are dissipated over longer times, thus reducing the light intensity's direct proportionality to stored energy.

DISCUSSION

We have demonstrated that a properly tailored cold collisional plasma significantly attenuates microwave radiation. The simultaneous reduction of direct backscatter, oblique backscatter, and cross-polarized scatter confirms that the effect is due to absorption rather than to conversion into other electromagnetic modes.

The spatial and temporal profiles of the plasma under study were governed by the distribution of photoionizing light intensity from the sparkboard sources, which varied as the inverse square of the distance from each individual spark, with additional attenuation with distance

due to absorption. The resulting peak electron densities had a Gaussian radial distribution at constant z and a variation with z that could be approximated by an Epstein profile. This distribution provided a gradual density gradient with scale length longer than the microwave wavelength as required to achieve low reflectivity. Although the distributions were not one-dimensional and although the peak electron densities near the source were not known, the measured microwave attenuation was in good agreement with predictions from a one-dimensional model calculated using the same scale length.

This work confirms the feasibility of switchable microwave absorbers based on cold collisional plasmas. Application of this technology will require more efficient ionization sources and ionization media.

Acknowledgment

This work was supported by the Plasma Physics Division of AFOSR under contract F49620-90-C-0041. We thank Bill Olson, Jr., for constructing some of the mechanical components and Steve Young for help with the pulsed power system. Gil Roach made the sparkboards and also lent us some of the microwave instrumentation for the high dynamic range measurements. Glen Tomlin assisted with the high dynamic range experiments.

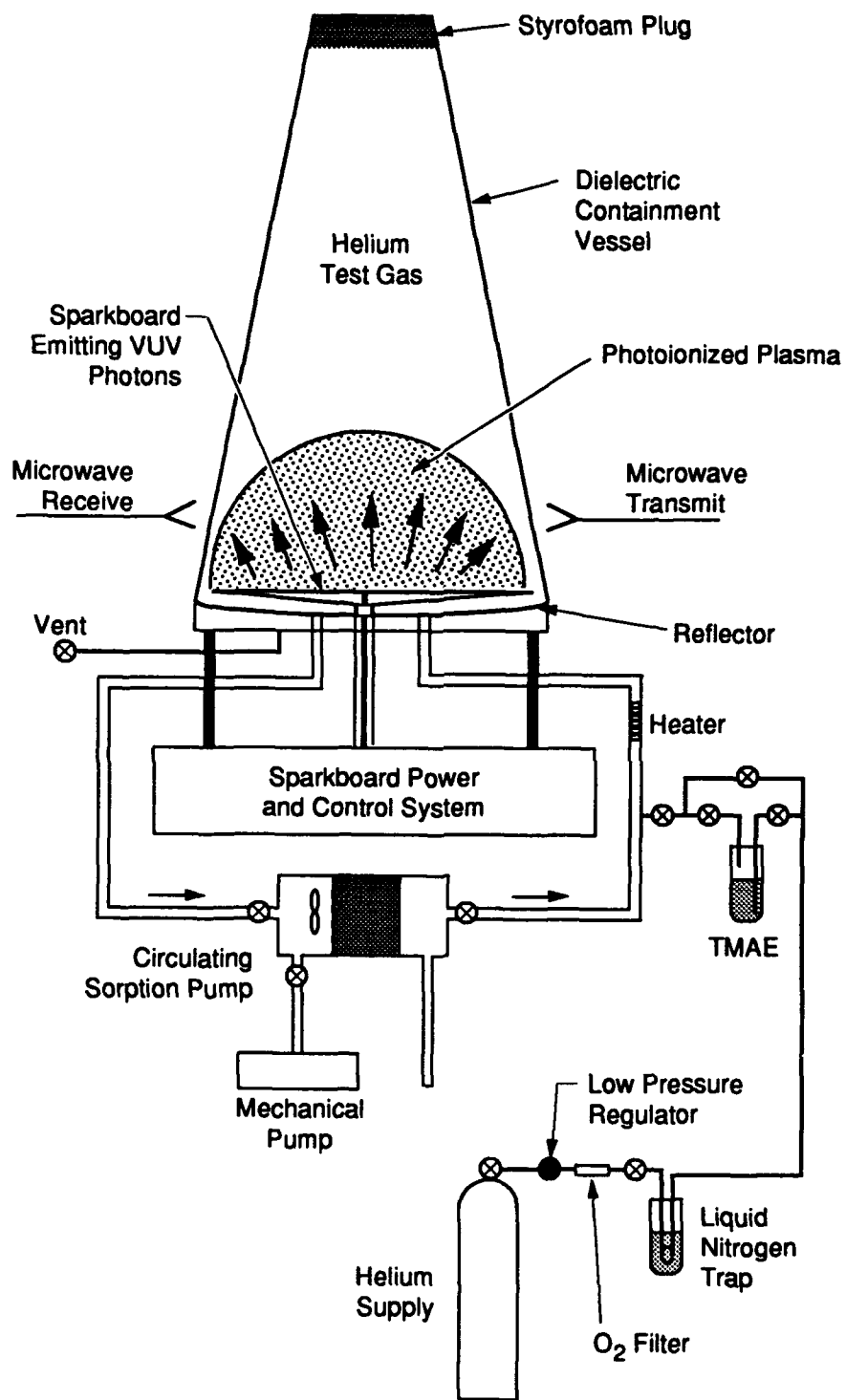
REFERENCES

1. R. J. Vidmar, *IEEE Trans. Plasma Sci.*, **18**, 733 (1990).
2. K. G. Budden, *The Propagation of Radio Waves*, Cambridge University Press, 1985.
3. H. C. Carlson, in *AGARD Conference Proceedings No. 485*, Paper 1B, Bergen, Norway, 28-31 May 1990.
4. W. W. Destler, J. E. DeGrange, H. H. Fleishmann, J. Rodgers, and Z. Segalov, *J. Appl. Phys.* **69**, 6313 (1991).
5. X. L. Zou, L. Laurent, and J. M. Rax, *Plasma Phys. Cont. Fusion* **33**, 903 (1991).
6. P. S. Epstein, *Proc. Nat. Acad. Sci., Wash.* **16**, 627 (1930).
7. K. R. Stalder and D. J. Eckstrom, submitted to *J. Appl. Phys.* (1992).
8. J. R. Woodworth, T. A. Green, and C. A. Frost, *J. Appl. Phys.* **57**, 1648 (1985).
9. H. J. J. Seguin, J. Tulip, and D. McKen, *Appl. Phys. Lett.* **23**, 344 (1973).
10. H. J. J. Seguin, J. Tulip, and D. McKen, *Appl. Phys. Lett.* **23**, 527 (1973).
11. D. F. Grosjean and P. Bletzinger, *IEEE J. Quantum Elect.* **QE-13**, 898 (1977)
12. M. C. Richardson, K. Leopold, and A. J. Alcock, *IEEE J. Quantum Elec.* **QE-9**, 934 (1973).
13. V. M. Borisov, G. G. Gladush, and Yu. Yu. Stepanov, *Sov. J. Quantum Elect.* **7**, 450 (1977).

14. R. E. Beverly III, *J. Appl. Phys.* **60**, 104 (1986).
15. D. M. Bartell, G. S. Hurst, and E. B. Wagner, *Phys. Rev. A* **7**, 1068 (1973)
16. P. C. Hill, *Phys. Rev. A* **40**, 5006 (1989).
17. C. M. Surko, R. E. Packard, G. J. Dick, and F. Reif, *Phys. Rev. Lett.* **24**, 657 (1970).
18. J. B. Tatum and W. A. Jaworski, *J. Quant. Spectrosc. Radiat. Transfer* **38**, 319 (1987).

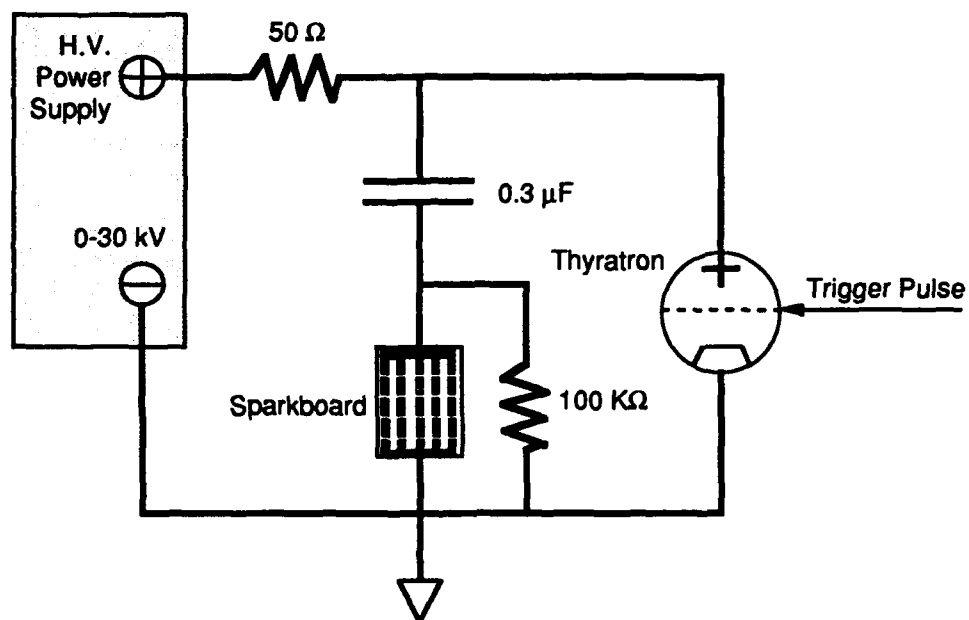
FIGURE CAPTIONS

- Figure 1. Diagram of the experimental apparatus.
- Figure 2. Diagram of the pulsed-power system used to drive the sparkboard array.
- Figure 3. Open shutter photograph of a single-sparkboard discharge with 30 spark gaps. A metal screen placed over the sparkboard causes the observed cross-hatching. The total energy discharged was 66 joules.
- Figure 4. Line-integrated electron density profiles for two sparkboard configurations and discharge conditions in TMAE-seeded helium. Square data points (experiment) and solid line (Gaussian fit): Four sparkboards; total energy of 49 joules, measured at $z = 16$ cm. Diamond-shaped data points (experiment) and dashed line (Gaussian fit): One sparkboard; total energy of 22 joules, measured at $z = 7$ cm.
- Figure 5. Model predictions of the total normal-incidence attenuation of microwaves in a plasma in atmospheric-pressure helium with an electron density scale length $\sigma = 5$ cm.
- Figure 6. Top view of the experimental layout for normal-incidence microwave absorption measurements in the anechoic chamber.
- Figure 7. Reduction in direct backscattered 10-GHz microwaves in TMAE-seeded helium. Four sparkboards discharged a total of 86 joules.
- Figure 8. Reduction in angular scattering of 10-GHz microwaves in TMAE-seeded helium. Four sparkboards discharged a total of 66 joules.
- Figure 9. Peak attenuation of normal-incidence 10-GHz microwaves versus sparkboard energy E . The attenuation varies as $E^{0.37}$.



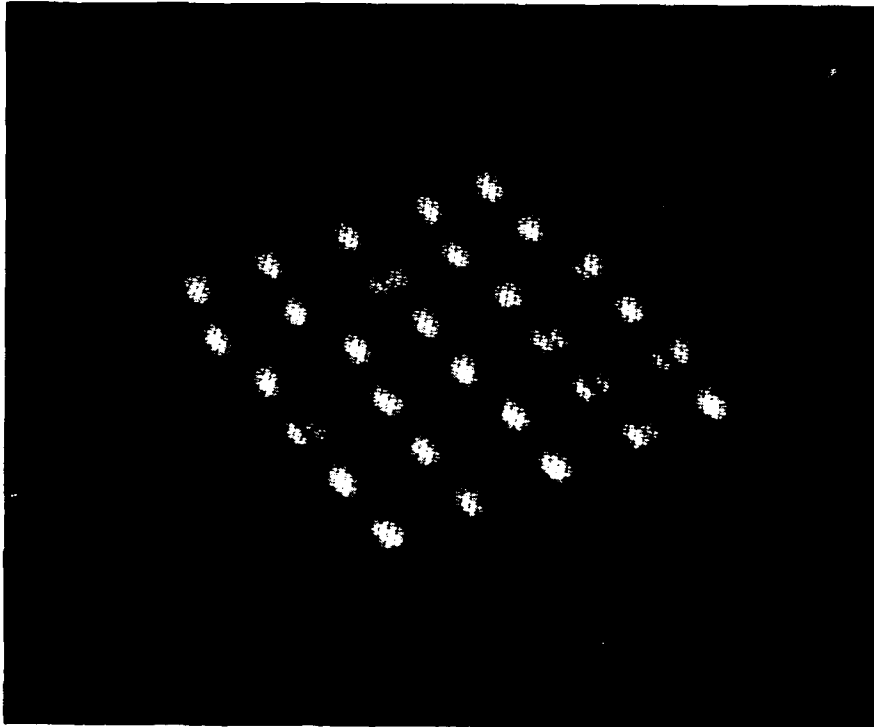
CAM-1261-1

Figure 1



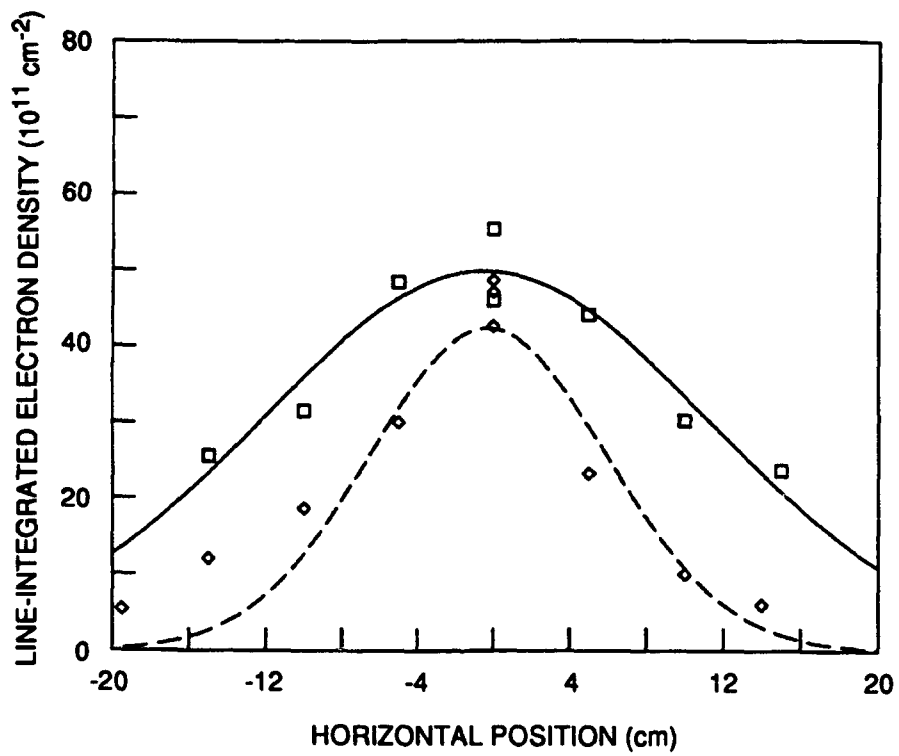
CAM-1261-2

Figure 2



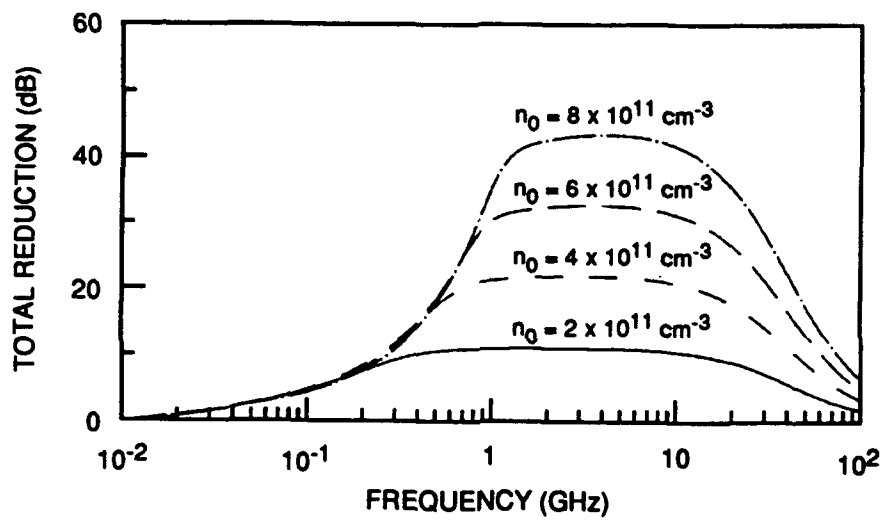
CP-1261-3

Figure 3



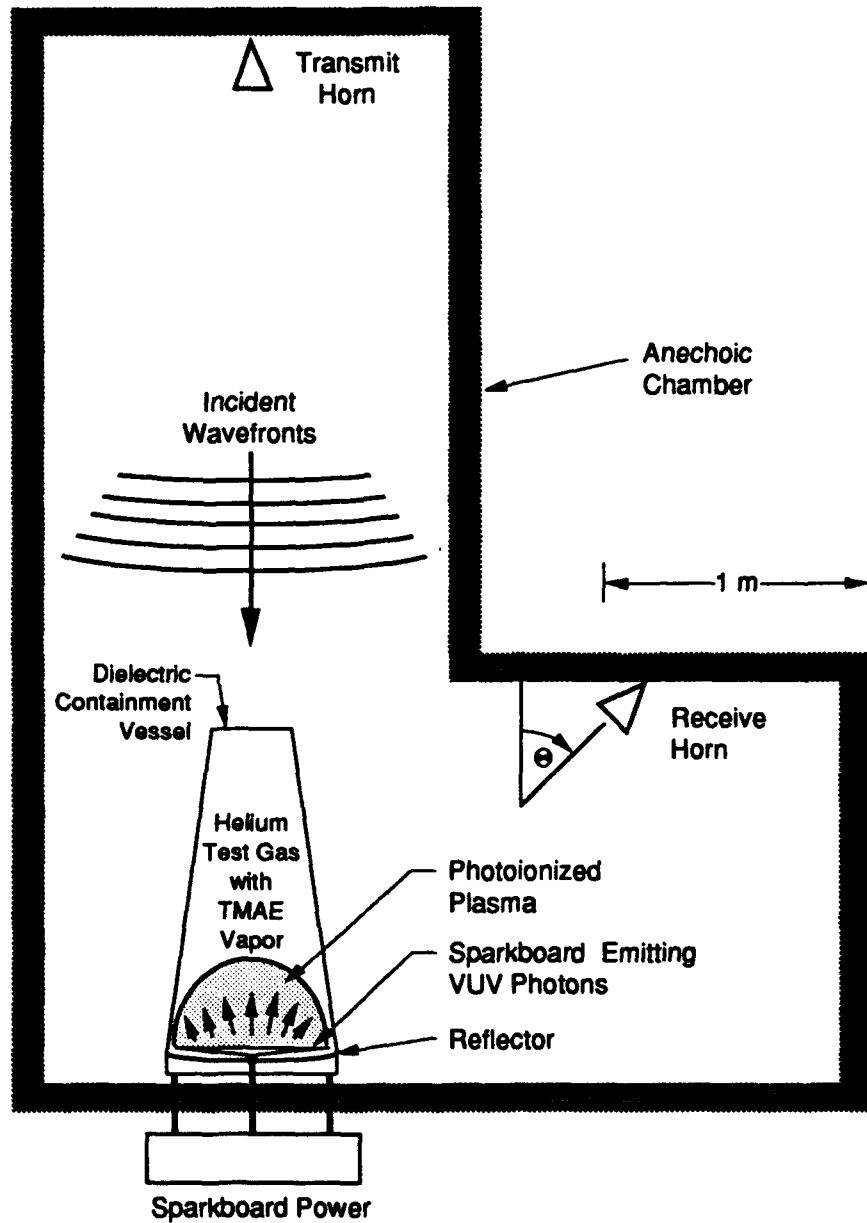
CM-1261-4

Figure 4



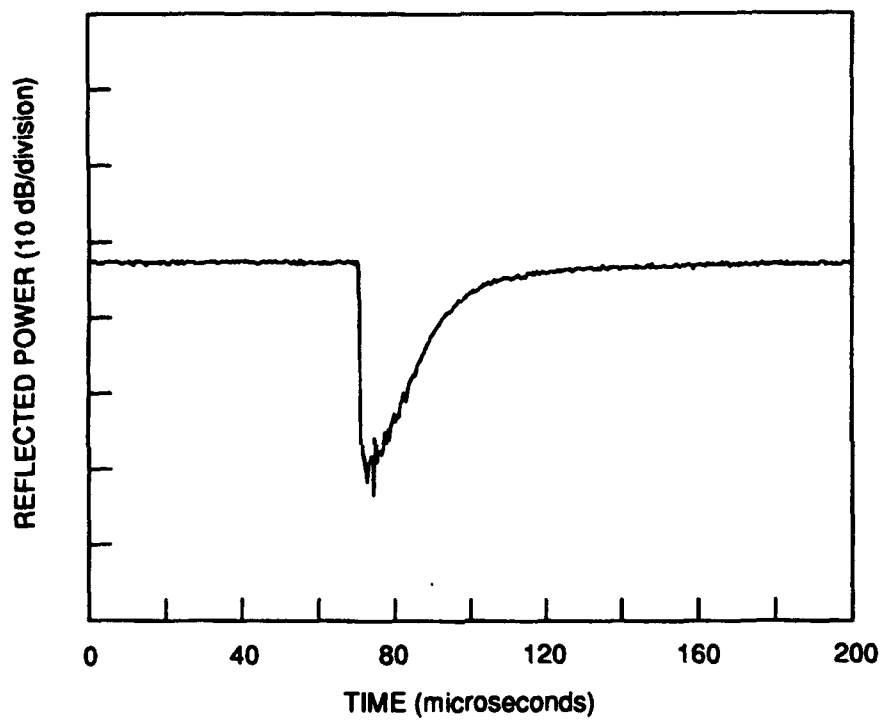
CM-1261-15

Figure 5



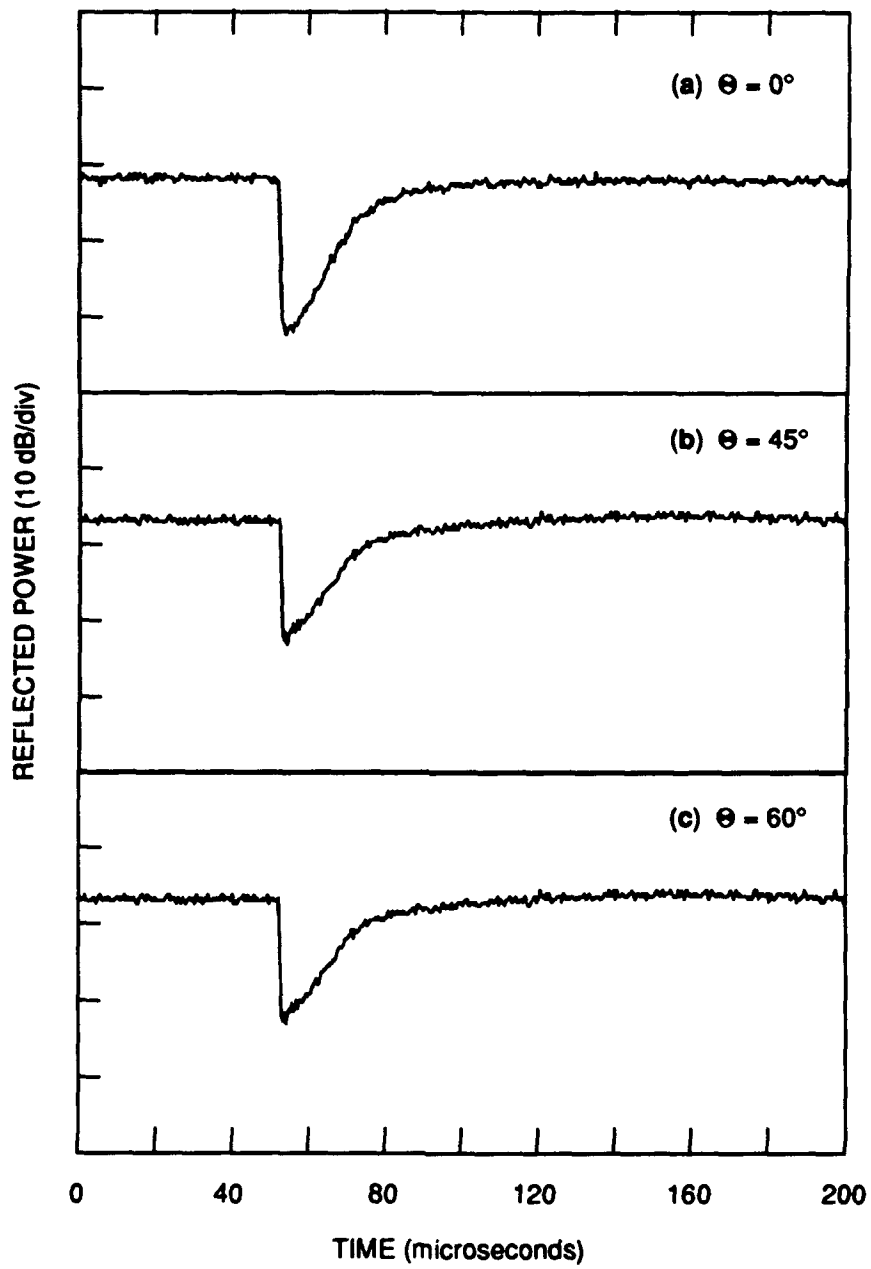
CAM-1261-6

Figure 6



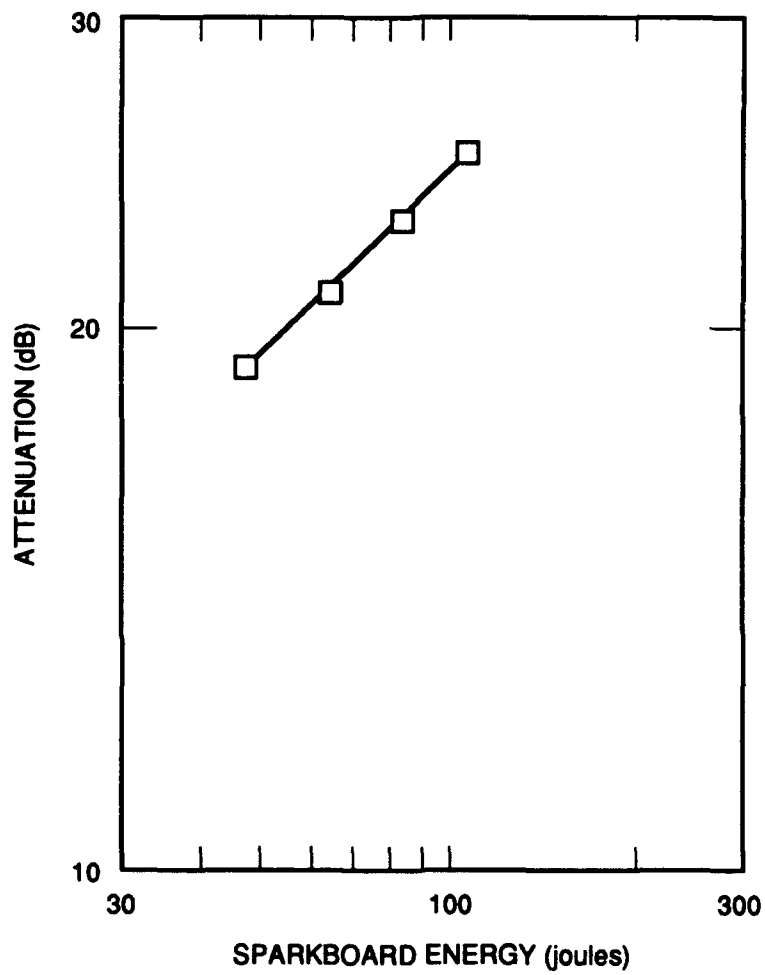
CM-1261-7

Figure 7



CM-1261-8

Figure 8



CM-1261-9A

Figure 9

Appendix B

**AFTERGLOW DECAY KINETICS OF NON-UNIFORM PLASMAS WITH
CYLINDRICAL SYMMETRY:
APPLICATION TO THE MEASUREMENT OF PLASMA DECAY IN LARGE,
PHOTOIONIZED PLASMAS IN ATMOSPHERIC-PRESSURE HELIUM**

K. R. Stalder and D. J. Eckstrom

To be Submitted to J. Appl. Phys. (1992).

**AFTERGLOW DECAY KINETICS OF NON-UNIFORM PLASMAS WITH
CYLINDRICAL SYMMETRY: APPLICATION TO THE MEASUREMENT OF
ELECTRON DECAY IN LARGE, PHOTOIONIZED PLASMAS IN
ATMOSPHERIC-PRESSURE HELIUM**

K. R. Stalder and D. J. Eckstrom
Molecular Physics Laboratory
SRI International
Menlo Park, CA 94025

PACS Numbers: 52.20.Fs, 52.40.Db, 34.80.Gs, 35.80.+s

ABSTRACT

Experiments and analytical methods for determining electron-ion recombination and attachment coefficients in highly collisional, cylindrically symmetric plasmas are presented. Photoionization by sparkboard light sources of tetrakisdimethylaminoethylene (TMAE) seeded in atmospheric-pressure helium is used to produce the plasma. The electron density is probed by microwave transmission techniques. The effective recombination coefficient for electrons recombining with TMAE ions in atmospheric pressure helium is found to be $(9.0 \pm 1.1) \times 10^{-6} \text{ cm}^3 \text{ s}^{-1}$ for $T_e = 300 \text{ K}$.

MP 92-013
April 14, 1992

INTRODUCTION

The afterglow decay of plasmas has been a topic of continuing interest for many years. Depending on details of the plasma environment, such as neutral gas species and densities and impurity concentrations, different functional forms describing the temporal decay are possible. For example, in plasmas that contain molecular ions, dissociative recombination is frequently important. Since this process is second-order, where the time scale of plasma decay depends on the electron density, the decay rate is relatively fast at high plasma densities. Three-body recombination, also second order, is important in some high pressure plasmas. In plasmas with significant concentrations of electron attaching species such as oxygen, attachment processes become important and since these are first-order, the time scale is independent of the electron density.

In connection with experiments on the microwave-absorption properties of highly collisional plasmas, we are studying the production and decay mechanisms of plasmas containing molecular ions that are produced in atmospheric-pressure helium. The present work is motivated by the potential application of collisional plasmas in creating large, switchable absorbers of microwave radiation.¹ The ions are created by the photoionization of tetrakisdimethylaminoethylene (TMAE), a low-ionization-potential, high-vapor-pressure molecule that is frequently used in Cerenkov detectors in high-energy physics experiments.^{2,3}

One of the goals of this research was to determine the plasma decay mechanisms so that reasonable physics-based extrapolations of the experimental results can be made. As a result of several experimental constraints, which are explained below, we had to consider the simultaneous effects of several decay processes in the analysis of the results. Electron-ion recombination by both dissociative and three-body processes was possible and indistinguishable. The helium also contained a non-negligible concentration of oxygen. Thus, we assume that the electron density

decay was influenced by at least two processes, electron-ion recombination and electron attachment.

The evolution of a plasma's spatial uniformity is also affected by the decay kinetics. Since recombination processes are second order, they result in nonlinear decay rates, and the resulting temporal and spatial evolution of the plasma density also is nonlinear. Because the ionization in the present experiments resulted in dense, non-uniform plasmas, these effects had to be included in our analysis of the afterglow kinetics.

The basic microscopic processes that describe the decay kinetics have been studied for many years. Dissociative recombination of electrons with molecular ions was authoritatively reviewed by Bardsley and Biondi⁴ and more recently by Johnsen.⁵ The kinetics of electron attachment were reviewed by Caledonia,⁶ and more recently by Gallagher et al.⁷ More specific to the present investigations, attachment of electrons to oxygen was most recently studied by Shimamori and Hotta.⁸ We are not aware of any previous studies of the recombination kinetics of TMAE. Methods for analyzing experimental measurements of recombination rates in non-uniform plasmas have also been extensively studied over the years.⁹⁻¹¹

This paper describes experimental details and our analytical approach to determining the afterglow kinetics of the plasma. We first review the basic kinetic equations applicable here. We then describe the microwave absorption technique of determining the electron density in uniform and non-uniform plasmas, followed by description of the experimental apparatus and constraints that led to this analysis. Finally, we use the results of the first two sections to determine the effective recombination and attachment rates that are applicable to this plasma.

SECTION 1

Afterglow Kinetics of Plasmas Subject to Dissociative Recombination and Electron Attachment

The decay of a plasma that is subject to electron-ion dissociative recombination, three-body recombination with helium acting as the third body, and attachment to impurity oxygen (with helium also acting as a third body to conserve energy and momentum) is described by the following equation:

$$dn_e/dt = -\alpha n_e^2 - \beta n_e^2 n_{He} - \lambda n_e n_{O_2} n_{He} \quad (1)$$

where n_e is the electron density, n_{He} is the helium density, n_{O_2} is the oxygen density, α is the two-body dissociative recombination coefficient for electrons recombining with molecular ions, β is the three-body recombination coefficient, and λ is the three-body attachment-rate coefficient for electrons attaching to oxygen molecules. Combining terms yields a simplified expression for n_e :

$$dn_e/dt = -\alpha' n_e^2 - \lambda' n_e \quad (2)$$

where $\alpha' \equiv \alpha + \beta n_{He}$ is the effective electron-ion recombination-rate coefficient, and $\lambda' \equiv \lambda n_{O_2} n_{He}$ is the effective attachment frequency.

The solution to Equation (2), which may be verified by substitution, is

$$n_e(0)/n_e(t) = \{[\alpha' n_e(0)/\lambda'] + 1\} \exp(\lambda' t) - \alpha' n_e(0)/\lambda' \quad (3)$$

where $n_e(0)$ is the initial electron density at $t = 0$.

Eq. (3) describes the evolution of the electron density at each point in the plasma, regardless of its uniformity, as long as $n_e(0)$ is interpreted as the initial local density. Although Eq. (3) is a general result, familiar simplifications may result if the relative contributions of the two terms on the right-hand side of Eq. (2) are strongly disparate. For example, if attachment is negligible ($\lambda' \rightarrow 0$), then Eq. (3) reduces to the well-known result:

$$n_e(t) = n_e(0)/[1 + \alpha'tn_e(0)]. \quad (4)$$

If electron-ion recombination is negligible ($\alpha' \rightarrow 0$), then Eq. (3) reduces to the familiar exponential-decay process:

$$n_e(t) = n_e(0)\exp(-\lambda't) \quad (5)$$

In the following sections we use the general result, Eq. (3), since our experimental conditions required consideration of both attachment and recombination processes.

SECTION 2

Microwave Absorption in Collisional Plasmas

The evolution of the plasma density in our experiments was probed by microwave transmission-absorption measurements. Microwave techniques, usually based on resonant-cavity perturbation methods, have been widely used to study plasma afterglows.^{4,9} We were prevented from applying the cavity method to the present experiments since the size of the plasma was too large and the electron density was too high to make accurate measurements using this technique. However, since the helium test gas was confined by a dielectric membrane, straightforward microwave transmission measurements were possible. We thus used an absorption measurement to determine the spatial and temporal evolution of the electron density. Since this technique is

sensitive to line-integrated spatial nonuniformities, the inhomogeneity of this plasma had to be measured and accounted for in the analysis of the afterglow decay. We discuss our method for analyzing the experimental measurements here.

The dispersion relation for electromagnetic waves with wavenumber k and frequency ω propagating in a cold collisional plasma can be written as

$$k^2 c^2 / \omega^2 = 1 - \omega_p^2 / \omega(\omega - i\nu) \quad (6)$$

where c is the speed of light, $\omega_p^2 = 4\pi e^2 n_e / m_e$ is the square of the electron plasma frequency, e and m_e are the charge and mass of the electron, respectively, and ν is the electron collision frequency. Usually the frequency ω is chosen to be real and k is allowed to be complex, in which case the real part, $k_r = 2\pi/\lambda$ [here λ is the wavelength of the wave] determines the wavelength and the imaginary part, k_i , represents the attenuation of the wave. It follows from Eq. (6) that when the electron collision frequency is very much greater than the plasma frequency and wave frequency, the attenuation of the wave is given as

$$k_i = -\frac{\omega_p^2}{2\nu c} \quad (7)$$

where the minus sign indicates exponential damping. In this case, the attenuation is linearly proportional to the electron density. Other conditions on the relative size of the three characteristic frequencies, ω , ν , ω_p , may also yield attenuation coefficients that are linear in the electron density, but for simplicity (and applicability to these experiments) we use the form given in Eq. (7).

The imaginary part of the wavenumber, k_i , which represents the attenuation of the wave, can be related to the total power absorption since the power is proportional to the square of the

electric field. For a slab geometry, the total absorption, A , is related to the integral of k_i over its path length, L . Thus,

$$A = \int_0^L k_i dx = \frac{1}{2} \ln(P_0/P) \quad (8)$$

where P and P_0 are the microwave transmitted power with and without the plasma, respectively. The factor of $\frac{1}{2}$ precedes the logarithm since k_i is the electric-field attenuation coefficient and the power is proportional to the square of the electric field.

Microwave Attenuation in Cylindrically Symmetric Plasmas

In the special case that the microwaves are transmitted along chords of a cylindrically symmetric plasma, the net attenuation of the beam is

$$A(y,t) = \zeta \int_{-\sqrt{a^2-y^2}}^{\sqrt{a^2-y^2}} n_e(r,t) dx = \frac{1}{2} \ln(P_0/P) \quad (9)$$

where the wave propagates in the x -direction, y represents the displacement of the probe beam with respect to the plasma centerline, a is the radius of the plasma, and ζ is a constant of proportionality. For the case described in the previous section, $\zeta = 4\pi e^2/2m_e v c$. Substituting Eq. (3) into Eq. (9), rearranging terms, and noting that the integrand is symmetric, the resulting attenuation becomes

$$A(y,t) = 2\zeta \int_0^{\sqrt{a^2-y^2}} n_e(r,0) dx / \{ [\alpha' n_e(r,0)/\lambda'] [\exp(\lambda't) - 1] + \exp(\lambda't) \} \quad (10)$$

where $x^2 + (y - y_0)^2 = r^2$; y_0 is a possible y -offset of the plasma with respect to the coordinate system.

Equation (10) for the recombination rate coefficient α' and the attachment frequency λ' is frequently solved by performing an explicit Abel inversion of the experimental attenuation data measured at many different y_i .¹² This procedure is required if no *a priori* information is known about the density profile, $n_e(r)$. If the spatial profile of the plasma density is known precisely, then the inversion of Eq. (10) is accomplished by a nonlinear least-squares fit of the absorption data, $A(y,t)$, as a function of t . For each y -value, the integral over x is computed numerically, with α' and λ' kept as free parameters; the remaining independent variable is the time, t . Then, the parameters α' and λ' are adjusted until the best-fit (χ^2 minimization procedure) of the temporal evolution of the data is obtained.

More commonly, the plasma profile is unknown, although its functional form may be known or estimated based on physical considerations. Parameters describing the density profile can then be kept as free parameters for the integration, and least-squares fitting procedures may be used to determine them. A particularly convenient and frequently encountered radial plasma profile is the Gaussian distribution, which for this analysis is defined as

$$n_e(r,0) = n_e(0,0)\exp(-r^2/2r_0^2), \quad (11)$$

where r_0 is a characteristic radius of the plasma. Converting to Cartesian coordinates and substituting Eq. (11) into Eq. (10) yields

$$A(y,t) = 2\zeta n_e(0,0) \exp\left(\frac{-y^2}{2r_0^2}\right) \int_0^\infty \frac{\exp\left(\frac{-x^2}{2r_0^2}\right) dx}{\left\{ \left[\frac{\alpha' n_e(0,0)}{\lambda'} \right] [\exp(\lambda' t) - 1] \left[\exp\left(\frac{-y^2}{2r_0^2}\right) \right] \left[\exp\left(\frac{-x^2}{2r_0^2}\right) \right] + \exp(\lambda' t) \right\}} \quad (12)$$

Here the upper limit of the integral in Eq. (12) has been increased to infinity since a Gaussian function remains finite as $x \rightarrow \infty$ and to simplify the integration. This simplification results in a negligible error in the present case. The integral equation for the attenuation contains two variables, y and t , and five initially unknown parameters, $n_e(0,0)$, r_0 , y_0 , α' , and λ' . By making absorption measurements along a number of (at least three, and preferably many more) chords, y_i , and evaluating the data at an arbitrarily chosen $t = 0$, we can determine the initial parameters $n_e(0,0)$, r_0 , and y_0 by a least-squares fit to the spatially varying absorption data, $A(y,0)$. Then, performing a least-squares fit of the temporal behavior of the absorption, we can determine the remaining unknown parameters, α' and λ' .

The parameters may also be determined by fitting the data in the opposite order. This is most readily seen by transforming Eq. (12) using the substitution $z^2 = \left(\frac{x^2}{2r_0^2}\right)$ and rearranging terms to get

$$A(y,t) = B(y)\exp(-\lambda't) \int_0^\infty \frac{\exp(-z^2)dz}{\left\{1 + \gamma(y) \frac{[1 - \exp(-\lambda't)]}{\lambda'} \exp(-z^2)\right\}} \quad (13)$$

where

$$B(y) = 2^{1/2} 2\zeta r_0 n_e(0,0) \exp\left[\frac{(y - y_0)^2}{2r_0^2}\right],$$

and

$$\gamma(y) = \alpha' n_e(0,0) \exp\left[\frac{(y - y_0)^2}{2r_0^2}\right].$$

Equation (13) is the integral equation to which we fit our experimentally measured absorption data in order to obtain the linear fitting parameter, $B(y)$, and the nonlinear parameters, $\gamma(y)$ and λ' . From the above definitions of each of these parameters, we note the following. First, $B(y)$ should vary as a Gaussian function of the offset y of the measurement chord with respect to the plasma centerline. By fitting $B(y)$ to a Gaussian, we can determine $n_e(0,0)$, r_0 , and y_0 .

Second, fitting $\gamma(y)$ to a Gaussian then enables us to determine the effective recombination coefficient, α' , since n_e is known from the prior fitting procedure. Third, the optimal value for the parameter that describes the effective attachment frequency, λ' , should not depend on the measurement chord.

For a total of N chordwise measurements, the total number of least-square fits required for this analysis is $N + 3$. That is, N fits of the temporal decay are required to obtain N values of $B(y)$, $\gamma(y)$, and λ' , and three additional fits of these parameters are required to obtain the spatial plasma density parameters, $n_e(0,0)$, τ_0 , y_0 , the effective recombination coefficient, α' , and the attachment rate frequency, λ' .

SECTION 3

Afterglow Decay of Photoionized TMAE in Helium Buffer Gases

As mentioned in the introduction, we are currently studying the interactions of microwaves with highly collisional plasmas formed by photoionizing TMAE admixed in atmospheric pressure helium.¹³ The plasma was produced in a thin plastic (Mylar) membrane in the shape of a conical frustum, 120 cm in height, that was mounted on a 60-cm-diameter aluminum baseplate and inflated with purified helium as shown schematically in Figure 1. Oxygen and residual impurities from air and other outgassing sources were removed in a custom-built recirculating sorption pump system that consisted of densely packed A5 zeolite cooled to near-liquid-nitrogen temperatures by a copper cold finger. Circulation was provided by a fan directly upstream of the zeolite so that oil vapor from the fan was also effectively removed. TMAE vapor was introduced downstream of the sorption pump and into the containment volume by bubbling helium through purified liquid TMAE maintained at constant temperature in an alcohol bath.

Although several photoionization sources have been tried with this experimental setup, the experiments described here were conducted using a single two-dimensional array of sparks aligned parallel to, and placed just above, the baseplate. Similar spark sources have been described for

their application to the large-area preionization of CO₂ lasers.^{14,15} Sparks generated by the discharge of a charged capacitor across a planar array of gaps in the thin-film metal strips produced a windowless, intense VUV light source that photoionized the TMAE. Each sparkboard (14 cm × 19 cm) contained 30 spark gaps arranged in 5 parallel current paths. The discharge was not critically damped, so the light usually oscillated in intensity for 3 to 5 μs, depending on discharge energy. All the present experiments were conducted with a modest 22 joules of discharge energy, which nevertheless resulted in a significant electron density. The resulting plasma extended quite far from the sparkboard, and its density depended strongly on the normal distance away from the sparkboard and on the lateral displacement from the centerline of the plasma.

The estimated time for electrons to thermalize to within 1% of the ambient gas temperature for photoelectrons with 10 eV initial energy is approximately 88 ns in helium at atmospheric density.¹⁶ Thus, it is safe to assume that the initial photoionized plasma was well thermalized to 300 K shortly after the light from the sparks terminated.

Measurements of the electron density produced by the sparkboard array were made with a 10-GHz microwave transmission apparatus. Transmit and receive horns were positioned such that measurements parallel to the baseplate could be made in horizontal and vertical planes. The collision frequency, ν , for 300 K electrons in 760-torr helium has been previously determined to be $1.8 \times 10^{11} \text{ s}^{-1}$.¹⁷ Thus, the condition on the relative magnitudes of relevant frequencies is $\nu^2 \gg \omega^2$, and the results of Section 1 are directly applicable to the analysis of these measurements. In this case, $\zeta = 2.90 \times 10^{-13} \text{ cm}^2$.

For a given height above the spark board, z , each spark contributes its own degree of ionization according to an inverse-square law, reduced by absorption, so the resulting net ionization for all sparks is not expected to follow an inverse square law profile near the board. It has proven to be sufficiently accurate in these experiments to model the ionization according to a Gaussian profile, as in Eq. (11), where r is the distance from the axis of symmetry of the cone. As

noted in Section 1, Gaussian profiles are particularly convenient because Abel inversion of the chord-integrated absorption is straightforward and yields radial distributions that are also Gaussian.¹²

A nonlinear least-squares fit of the experimental absorption data taken 7 cm above the sparkboard to a Gaussian profile is shown as a solid line in Fig. 2. This procedure yielded a maximum on-axis density at $z = 7$ cm at the peak of the plasma profile (while the light from the sparkboard was at its maximum intensity) of $n(0,0) = 1.6 \times 10^{11} \text{ cm}^{-3}$. The plasma radius was $r_0 = 6.8 \text{ cm}$.

The afterglow period, following cessation of the photoionization by the light from the sparks, began in this case $3.2 \mu\text{s}$ after firing the sparkboard. Figure 3 presents the absorption data near the plasma centerline ($y - y_0 \sim 0$) and the fit determined by the methods described in the previous sections. Figure 3a shows the logarithm of the attenuation; if recombination were not a factor (i.e., $\alpha' = 0$), the fit would be a straight line in this representation. Figure 3b shows the reciprocal attenuation, which would be represented by a straight line if attachment was negligible (i.e., $\lambda' = 0$). We see that neither attachment nor recombination dominates over the entire time scale of the measurement, and thus the full treatment described by Eq. (13) must be applied to accurately describe the recombination kinetics. Physically, these results mean that a nonnegligible amount of oxygen was present in the plasma, and this oxygen was an effective scavenger of electrons. At early times however, electron-ion recombination was dominant.

Figures 4 and 5 show the spatial dependence of the parameters $B(y)$ and $\gamma(y)$, and the least-square fits according to their Gaussian definitions. We see that both $B(y)$ and $\gamma(y)$ are reasonably well described by Gaussian functions. The effective recombination rate for TMAE was thus determined to be $\alpha' = (9.0 \pm 1.1) \times 10^{-6} \text{ cm}^3 \text{ s}^{-1}$. We stress that this is an effective rate because the experimental constraints prevented us from varying the helium pressure from atmospheric pressure, and thus we cannot determine the relative contributions from true two-body dissociative recombination and three-body recombination.

Figure 6 shows that the attachment frequency, λ' , is also reasonably constant, except for several points near the sparkboard ($z = 7$ cm), which deviate significantly from the others. Three of the eight data points taken at this height are within the statistical error of the mean. We are not certain of the origin of the rather poor agreement of the outlying data points. We believe that some of the discrepancy may be due to scattering of the probe microwaves near the sparkboard. Farther away from the sparkboard, where scattering was negligible, the attachment-rate coefficients are well-clustered about a constant value. The effective attachment frequency, $\lambda' = \lambda n_{O_2} n_{He}$, was thus determined to be $\lambda' = (1.0 \pm 0.4) \times 10^5 \text{ s}^{-1}$.

Since the helium was maintained at atmospheric pressure, which corresponds to $n_{He} = 2.5 \times 10^{19} \text{ cm}^{-3}$, and knowing that the three-body attachment rate⁸ for 300 K electrons to oxygen in helium is $(3.3 \pm 0.3) \times 10^{-32} \text{ cm}^6 \text{ s}^{-1}$, we deduce that the oxygen density was approximately $1.2 \times 10^{17} \text{ cm}^{-3}$, or approximately 0.5% of the ambient helium density. We believe that the relatively high concentration of oxygen was a consequence of the rather inefficient method of gas scrubbing. Nevertheless, the oxygen concentration was reduced to levels that allowed photoionization to occur far from the sparkboard and also made measurements of the recombination possible.

DISCUSSION

Although the physical and chemical properties of TMAE have been studied for quite some time, the present measurement constitutes the first known for its recombination coefficient. The recombination rate for TMAE is larger than that for simpler polyatomic molecules like N_4^+ [$2 \times 10^{-6} \text{ cm}^3 \text{ s}^{-1}$] but comparable to that for complex polyatomic molecules like benzene. In fact, studies of the dissociative recombination rate of the benzene ion ($C_6H_6^+$), another large organic molecule, indicate a value for α that is comparable to that of TMAE⁺. Eckstrom et al.^{18,19} report that the dissociative recombination rate for benzene is $8 \times 10^{-6} \text{ cm}^3 \text{ s}^{-1}$ at $T_e = 300 \text{ K}$. Thus, the currently measured value for the recombination rate for TMAE is slightly larger than benzene's. This result seems reasonable based on the large size of TMAE (molecular weight= 200 amu) and

its probable large number of vibrational degrees of freedom that may result in dissociation upon electron capture. Also, three-body processes may play some role in our measurements, but their contribution to the recombination will have to be determined in another experiment.

Electron attachment to TMAE, forming negative ions, is believed to be insignificant since TMAE is a strong electron donor. Although the electron affinity of TMAE is unknown, its attachment rate is believed to be small because the electron mobility in liquid TMAE is large.²⁰

Another factor that complicates the conclusions to be drawn from the present experiments is that photodissociation may also accompany photoionization. Photoionization of large polyatomic molecules does not necessarily result in a single parent ion species and may result in many different fragment ions.²¹ For high-intensity multiphoton ionization of benzene at 248 nm, these effects can be quite large. However, at low two-photon photoionization fluxes of 2.3×10^6 W/cm², Rossi and Eckstrom²² report that 95% of the total benzene photoions are parent ions. In single-photon processes where the photon energies are high enough to access the many different dissociating potential curves that probably exist for complicated molecules like benzene and TMAE, fewer ions may be unfragmented. For example, at photon energies of 21.2 eV, which is 12 eV above the first ionization potential of benzene, only approximately 44% of the total ions are parent ions for single-photon photoionization.²¹ The spectral distribution of light from the sparkboard is unknown, but is certainly broader than for laser photoionization sources. Details regarding the dissociation pathways during photoionization of TMAE are unknown, and thus it is impossible to predict the ion species distribution in the present experiments, but we presume that our measured recombination rate is for the simple TMAE⁺ ion.

SUMMARY

It has been shown that, in the special case of cylindrically symmetric Gaussian plasma profiles, the recombination and attachment rates of a highly collisional plasma may be quantitatively determined by measuring the time and space dependence of the absorption of microwaves along chords intersecting the plasma. The observed rate of decay of the line-of-sight integrated absorption decreases as a Gaussian function with increasing displacement of the measurement chord from the centerline.

Using this method, we measured the effective recombination rate for TMAE⁺ ions to be $(9.0 \pm 1.1) \times 10^{-6} \text{ cm}^3 \text{ s}^{-1}$ for $T_e = 300 \text{ K}$.

ACKNOWLEDGMENTS

Very fruitful discussions and help with the nonlinear fitting procedures, provided by Dr. David L. Huestis, are gratefully acknowledged. Dr. Rainer Johnsen also provided useful insights into the interpretation of the afterglow decay. In addition to participating in stimulating discussions, Dr. Robert Vidmar provided the plastic containment membrane and aluminum baseplate. This work was supported by AFOSR under contract number F49620-90-C-0041.

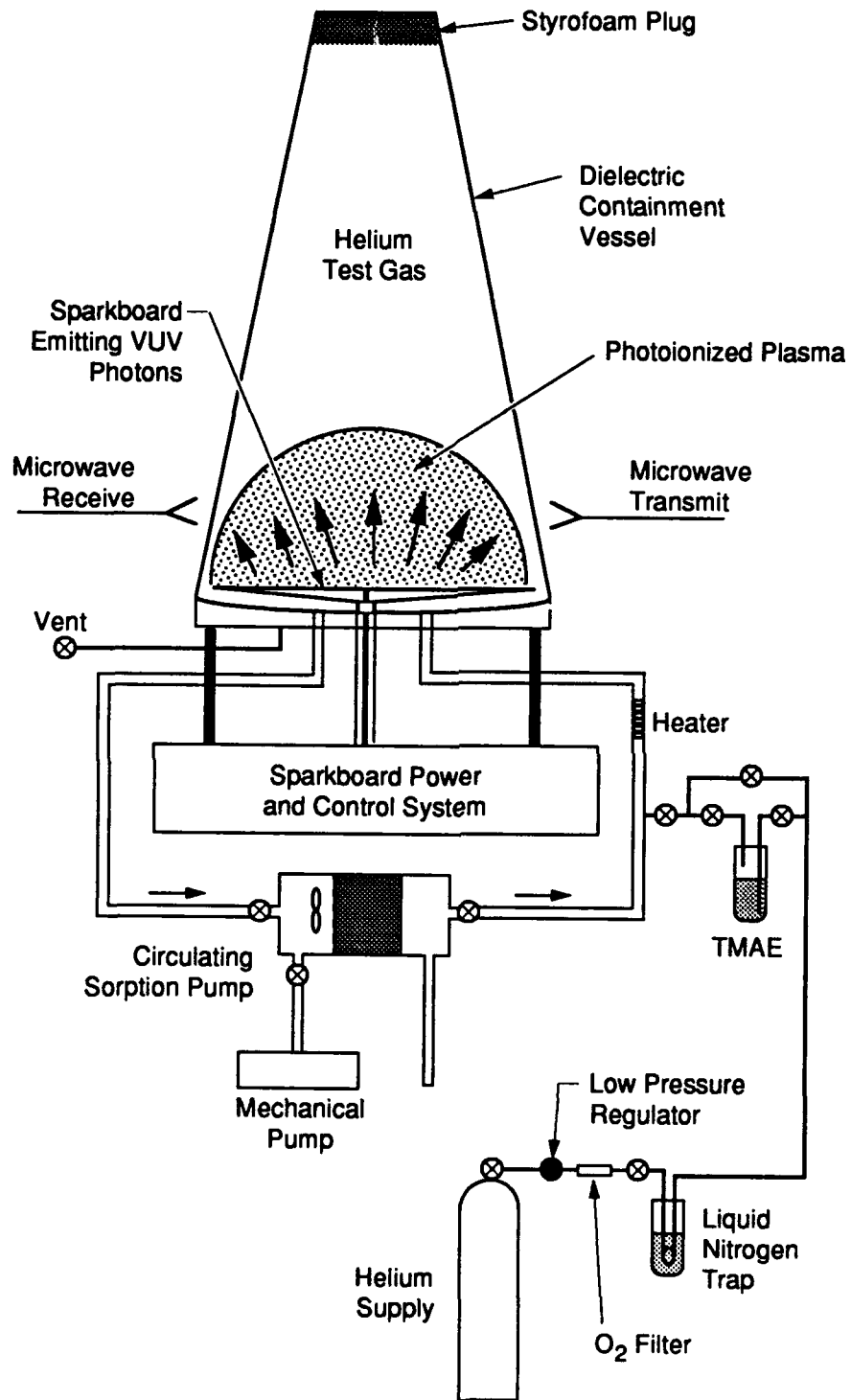
REFERENCES

1. R. J. Vidmar, *IEEE Trans. Plasma Sci.* **18**, 733 (1990)
2. D. F. Anderson, *Phys. Lett.* **118B**, 230 (1982)
3. R. T. Rewick, M. L. Schumacher, S. L. Shapiro, T. B. Weber, M. Cavalli-Sforza, *Anal. Chem.* **60**, 2095 (1988).
4. J. N. Bardsley and M. A. Biondi, in *Advances in Atomic and Molecular Physics*, Vol. 6, p. 1, Academic Press, New York, 1970.
5. R. Johnsen, *Int. J. Mass Spectrosc. Ion. Proc.* **81**, 67 (1987)
6. G. E. Caledonia, *Chem. Reviews* **75**, 333 (1975)
7. J. W. Gallagher, E. C. Beaty, J. Dutton and L. C. Pitchford, *J. Phys. Chem. Ref. Data* **12**, 109 (1983).
8. H. Shimamori and H. Hotta, *J. Chem. Phys.* **81**, 1271 (1984)
9. L. Frommhold and M. A. Biondi, *Ann. Phys.* **48**, 407 (1968)
10. E. P. Gray and D. E. Kerr, *Ann. Phys.* **17**, 276 (1962).
11. R. F. Whitmer, *Phys. Rev.* **104**, 572 (1956).
12. J. B. Tatum and W. A. Jaworski, *J. Quant. Spectrosc. Radiat. Transfer* **38**, 319 (1987).

13. K. R. Stalder, D. J. Eckstrom, and R. J. Vidmar, Conference Record, 1991 IEEE International Conference on Plasma Science, Paper 1A7, p. 87, June 3-5 (1991) (unpublished).
14. M. C. Richardson, K. Leopold, and A. J. Alcock, IEEE J. Quantum Elec. **QE-9**, 934 (1973)
15. V. M. Borisov, G. G. Gladush, and Yu. Yu. Stepanov, Sov. J. Quantum Elec. **7**, 450 (1977).
16. A. Mozumder, J. Chem. Phys. **72**, 1657 (1980).
17. Y. Itikawa, Phys. Fluids **16**, 831 (1973)
18. D. J. Eckstrom, K. R. Stalder, and M. S. Williams, "Diagnostics Development for E-Beam Excited Air Channels," SRI Report 90-003 (12 February 1990).
19. D. J. Eckstrom, J. S. Dickinson, and M. N. Spencer, Proceedings of the 39th Annual Gaseous Electronics Conference, Paper CA-8, p. 46, Madison, WI, Oct 7-10 (1986), (unpublished).
20. R. A. Holroyd, S. Ehrenson, and J. M. Preses, J. Phys. Chem. **89** 4244 (1985).
21. J. Berkowitz, *Photoabsorption, Photoionization and Photoelectron Spectroscopy*, Academic Press, New York, 1979.
22. M. Rossi and D. J. Eckstrom, Chem. Phys. Lett. **120**, 118 (1985).

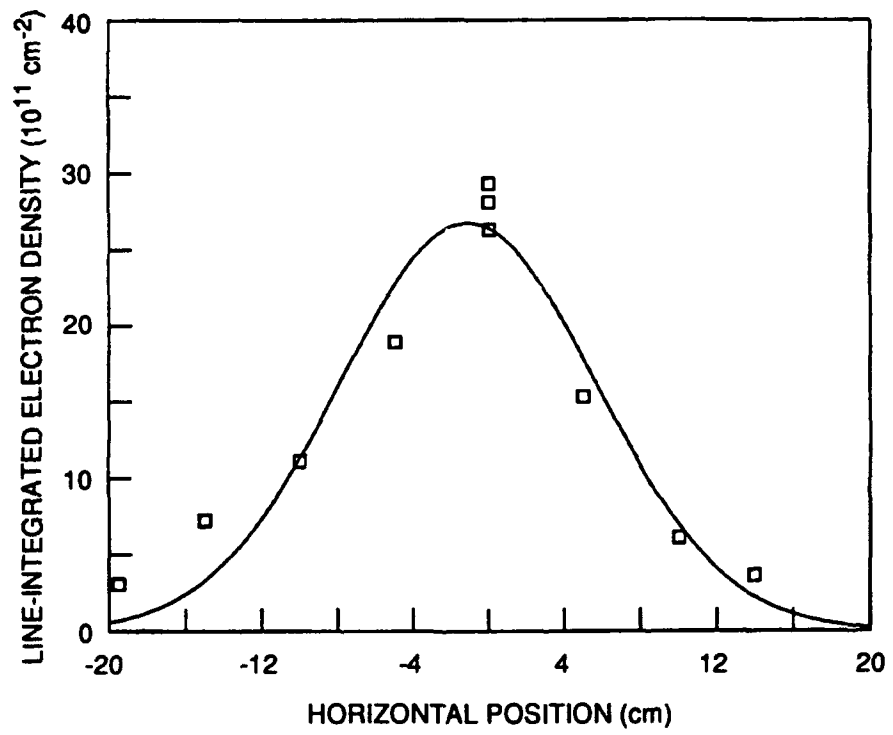
FIGURE CAPTIONS

- Figure 1. Diagram of the photoionization and afterglow-decay experiment.
- Figure 2. Experimentally measured integrated line-density of photoionized plasma (square data points) and Gaussian-fitted profile (solid line) at $z = 7$ cm while the light from the sparkboard was at its maximum intensity.
- Figure 3. Absorption data near the plasma centerline.
(a) Logarithm of the chord-integrated attenuation, $\ln(A)$, (square data points), versus time along the plasma centerline ($y = 0$), for $z = 7$ cm above the sparkboard. The solid line results from a nonlinear least-squares fit of the attenuation data to Eq. (13).
(b) Reciprocal attenuation, A^{-1} , (square data points), versus time for the same data shown in Fig. 3a. The solid line is also from the least-squares fit of the attenuation data to Eq. (13).
- Figure 4. Experimental values (squares) and Gaussian fit for the linear coefficient, $B(y)$, in Eq. (13)
- Figure 5. Experimental values (squares) and Gaussian fit for the nonlinear coefficient, $\gamma(y)$, in Eq. (13)
- Figure 6. Experimental values for the attachment rate coefficient, λ' , versus y for three heights above the sparkboard. Closed circles, $z = 7$ cm. Open circles, $z = 16$ cm. Solid squares, $z = 24$ cm.



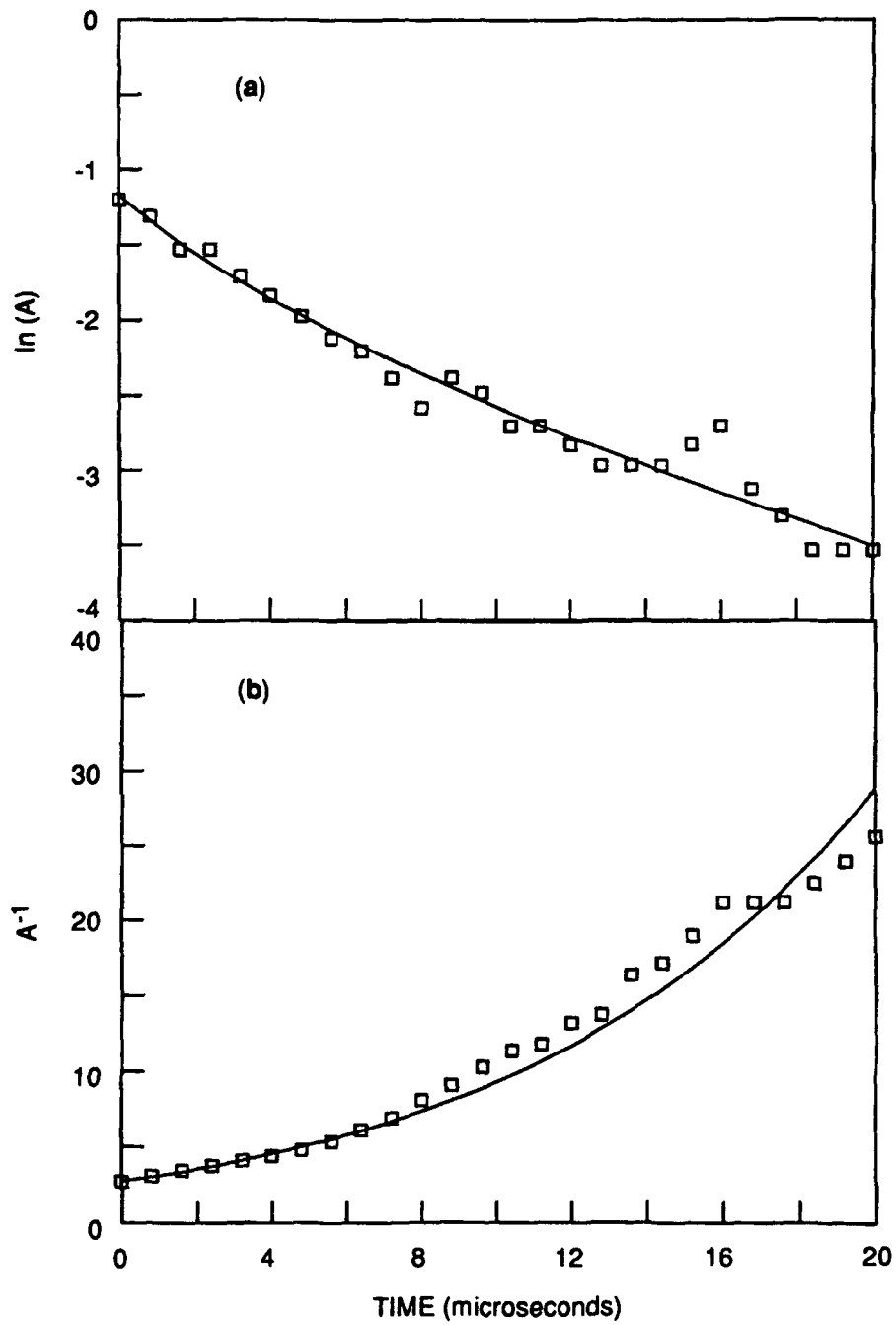
CAM-1261-1A

Figure 1



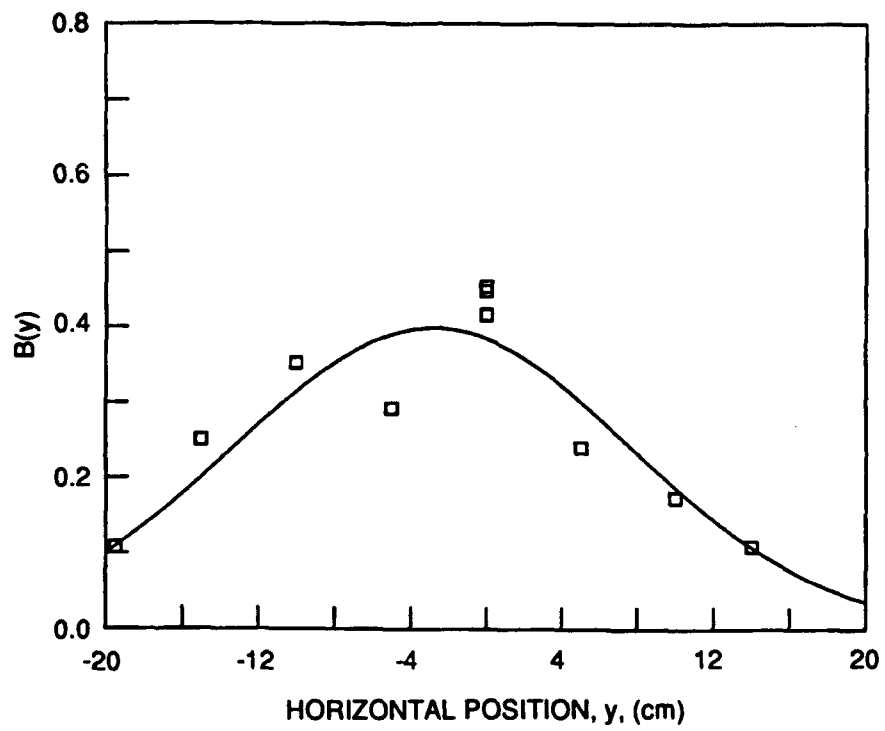
CM-1261-10

Figure 2



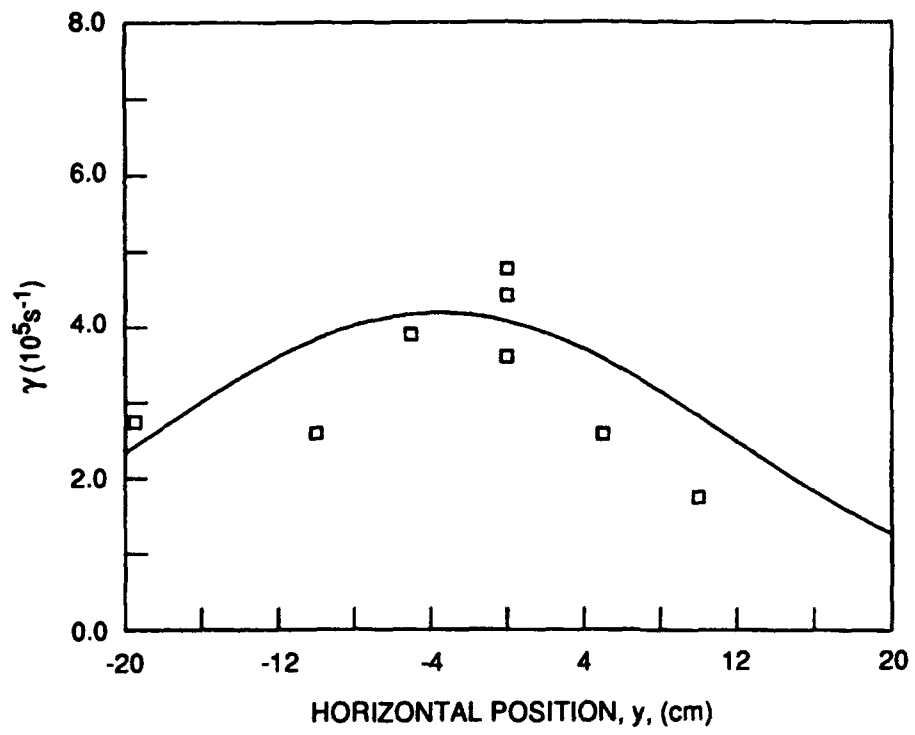
CM-1261-11

Figure 3



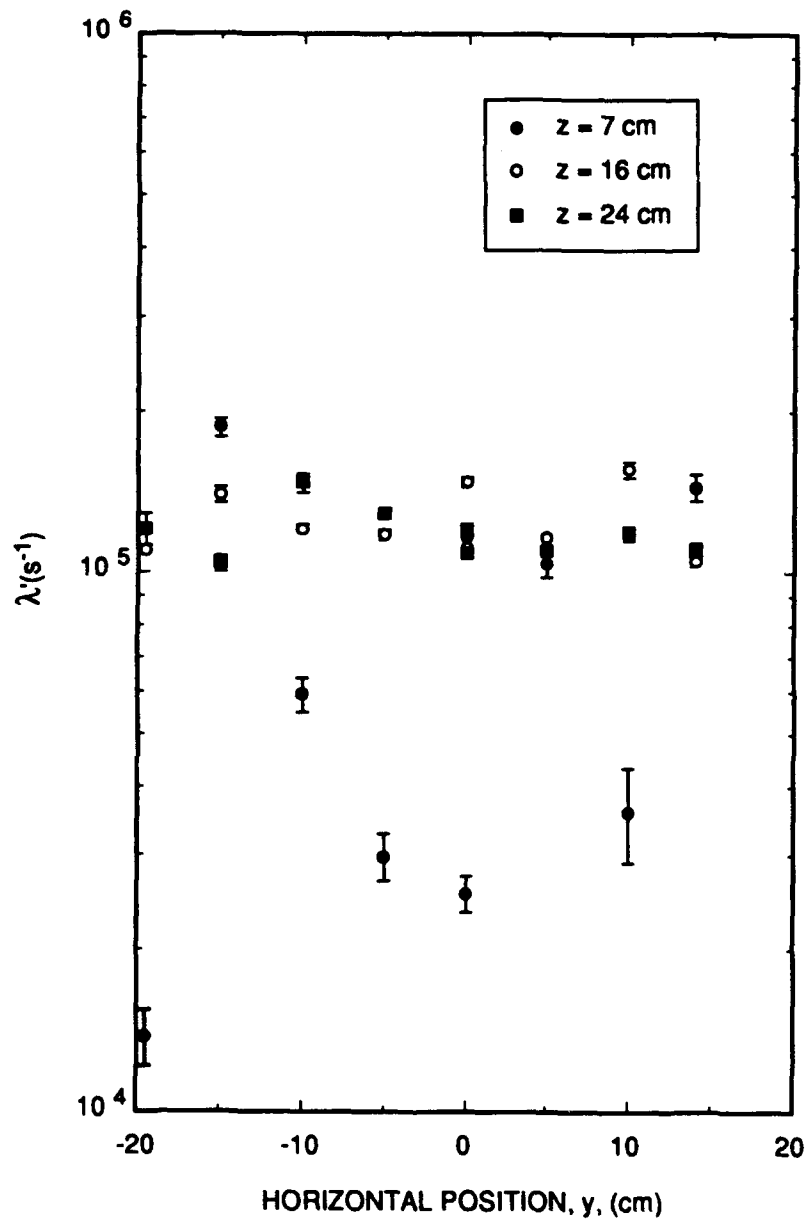
CM-1261-12

Figure 4



CM-1261-13

Figure 5



CAM-1261-14

Figure 6

Appendix C

**INVESTIGATIONS OF EFFICIENT PHOTOIONIZATION METHODS FOR
CREATING HIGHLY COLLISIONAL PLASMAS**

K. R. Stalder, D. J. Eckstrom and R. J. Vidmar

**Presented at the 43rd Annual Gaseous Electronics Conference, Champaign-Urbana, IL,
16-19 October 1990.**

INVESTIGATIONS OF EFFICIENT PHOTOIONIZATION METHODS FOR CREATING HIGHLY COLLISIONAL PLASMAS*

**K. R. Stalder, D. J. Eckstrom and R. J. Vidmar
SRI International, Menlo Park, CA**

We are beginning a program designed to investigate microwave absorption in highly collisional plasmas. Considerable effort will be placed on developing means for efficiently ionizing large volumes of high pressure gases. Our initial experiments will utilize two-dimensional, windowless spark-board arrays in helium. Two-step photoionization by resonance radiation will create a highly collisional plasma with a tailored electron density gradient which should absorb microwaves over a large bandwidth. Addition of low-ionization-potential additives will enhance the ionization yield. Plasma densities and collision frequencies will be determined from measurements using Langmuir probes and microwave interferometers. We will report our results for the spark-board experiments and on the plasma density profiles generated by these light sources.

*Work Supported by AFOSR under Contract No. F49620-90-C-0041.

Appendix D

**MICROWAVE-PLASMA INTERACTIONS IN PHOTOIONIZED, TMAE-SEEDED
HELIUM GAS MIXTURES**

K. R. Stalder, D. J. Eckstrom and R. J. Vidmar

**Presented at the 1991 IEEE International Conference on Plasma Science, Williamsburg, VA
3-5 June 1991**

MICROWAVE-PLASMA INTERACTIONS IN PHOTOIONIZED, TMAE-SEEDED HELIUM GAS MIXTURES*

K. R. Stalder, D. J. Eckstrom and R. J. Vidmar

Molecular Physics Laboratory
SRI International
Menlo Park, CA 94025

We report on experimental measurements of the microwave attenuation in highly collisional plasmas created by the photoionization of tetrakis-dimethylamino-ethylene (TMAE) mixed in atmospheric pressure helium contained in a conical frustum, thin-film-mylar vessel. Separate experiments, examining microwave interactions from two different photoionization sources, were performed. The sources were placed near the bottom baseplate consisting of 60-cm diameter, 360-cm focal length aluminum reflector. Best results for peak microwave attenuation were achieved with a windowless, two-dimensional spark array dissipating total energies as high as 135 Joules in 10 μ s. This light source is expected to generate substantial energy in the vacuum ultraviolet (VUV), peaking at 80 nm, thus efficiently ionizing TMAE (ionization potential=5.4 eV). Lower ionization levels, although lasting for significantly longer durations, were achieved with modified commercial, high-energy flashtubes dissipating as much as 2400 Joules.

Microwave probing of this collisional plasma was at a frequency of 9.60-GHz. Measurements of the direct transmission across radial chords that were at constant heights above the baseplate yield line-integrated electron densities and radial profiles. The transmission coefficient as a function of height above the baseplate yields the axial gradient of plasma density. Peak plasma densities as high as $6 \times 10^{10} \text{ cm}^{-3}$ 12 cm above the sparkboard have been achieved. Measurements of the plasma density decay time from short-pulse sparkboard ionization indicates the electron kinetics in TMAE are dominated by a relatively fast dissociative recombination coefficient of $4 \times 10^{-6} \text{ cm}^3\text{sec}^{-1}$.

Langmuir probe measurements of the plasma density have also been made. Absolute measurements using collisional probe theory indicate much higher plasma densities than those measured by the microwave attenuation technique, although the decay times observed with the probe are consistent with the microwave measurements.

Efforts are currently concentrated on improving gas purity levels; oxygen contamination adversely limits the plasma lifetime as well as decreases the spatial plasma gradient scale lengths due to absorption of the VUV radiation. Also, characterization of the VUV-spectral output of the spark board is underway. Measurements of the normal incidence attenuation, and bi-static back-scattering and polarization changes over larger microwave bandwidths are planned and initial results will be reported.

*This work is supported by the AFOSR under Contract No. F49620-90-C-0041.

Appendix E

DISSOCIATIVE RECOMBINATION OF TMAE IONS

K. R. Stalder, D. J. Eckstrom and R. J. Vidmar

**Presented at the 44th Annual Gaseous Electronics Conference, Albuquerque, NM
22-25 October 1991**

DISSOCIATIVE RECOMBINATION OF TMAE IONS*

K. R. Stalder, D. J. Eckstrom and R. J. Vidmar
SRI International, Menlo Park, CA

Experiments on microwave absorption in highly collisional plasmas created by the photoionization of tetrakis-dimethylamino ethylene (TMAE) vapor in atmospheric pressure helium are being conducted. The lifetime of the plasma, approximately 20 μ s, is controlled by dissociative recombination of electrons with the TMAE ions. Electrons are quickly thermalized to 300 K. The plasma is fairly large (10's of cm) and nonuniform with an approximate Gaussian density profile. Microwave transmission experiments probing the plasma density profile have been conducted. Peak plasma densities as high as $1.6 \times 10^{11} \text{ cm}^{-3}$ have been observed. The dissociative recombination coefficient of TMAE ions with 300 K electrons in this nonuniform plasma has thus been determined to be $(9.7 \pm .6) \times 10^{-6} \text{ cm}^3 \text{ s}^{-1}$.

*Work supported by AFOSR Contract No. F49620-90-C-0041.

Appendix F

**MICROWAVE ABSORPTION CHARACTERISTICS OF AN ATMOSPHERIC-
PRESSURE, PHOTOIONIZED PLASMA**

K. R. Stalder, D. J. Eckstrom, and R. J. Vidmar

Presented at the 1991 Annual Meeting of the APS Division of Plasma Physics, Tampa FL

4-8 November 1991.

Also published in Bull. Am. Phys. Soc., **36**, 2485 (1991).

MICROWAVE ABSORPTION CHARACTERISTICS OF AN ATMOSPHERIC-PRESSURE, PHOTOIONIZED PLASMA*

K. R. Stalder, D. J. Eckstrom and R. J. Vidmar
SRI International, Menlo Park, CA

We report on experimental measurements of the microwave absorption in highly collisional plasmas created by the photoionization of low-ionization potential organic molecules seeded in atmospheric pressure helium. The photoionization source, a two-dimensional spark array, was located on the bottom baseplate which also served as a 60-cm diameter, 360-cm focal length reflector.

The radial density profile, determined by transverse microwave probing, was established to be nearly Gaussian-shaped, and the plasma density decayed nearly exponentially from the light source in the normal direction. Peak plasma densities as high as $1.6 \times 10^{11} \text{ cm}^{-3}$ 16 cm above the sparkboard have been achieved. Dissociative recombination controls the plasma decay kinetics.

Normal-incidence backscattering measurements have demonstrated at least 29 dB of attenuation at 10.0-GHz. Polarization rotation is negligible, at least in direct backscattering. Efforts are underway to examine the sidescattering to see if any energy is scattered into other directions. These results are analyzed in terms of collisional absorption theory in non-uniform plasmas.

*Work supported by AFOSR, Contract No. F49620-90-C-0041.